Universidade do Minho
Escola de Engenharia

Ana Isabel Magalhães Marinho

Development of a force scaling method for upper body musculoskeletal models to estimate muscle fatigue

Dissertação de Mestrado
Mestrado Integrado em Engenharia Biomédica
Ramo Biomateriais, Reabilitação e Biomecânica

Trabalho efetuado sob a orientação do(a)
Professor Doutor Eurico Seabra
Professora Doutora Cristina Santos

maio de 2023

DIREITOS DE AUTOR E CONDIÇÕES DE UTILIZAÇÃO DO TRABALHO POR TERCEIROS

Este é um trabalho académico que pode ser utilizado por terceiros desde que respeitadas as regras e boas práticas internacionalmente aceites, no que concerne aos direitos de autor e direitos conexos.

Assim, o presente trabalho pode ser utilizado nos termos previstos na licença abaixo indicada.

Caso o utilizador necessite de permissão para poder fazer um uso do trabalho em condições não previstas no licenciamento indicado, deverá contactar o autor, através do RepositóriUM da Universidade do Minho.

Licença concedida aos utilizadores deste trabalho

Atribuição-NãoComercial-SemDerivações
CC BY-NC-ND

https://creativecommons.org/licenses/by-nc-nd/4.0/

Acknowledgments

I would like to express my deepest gratitude to my advisors, Professor Eurico Seabra and Professor Cristina Santos for their support, guidance, and availability. I am grateful for respecting my opinions and for the trust placed throughout the realization of this project.

This endeavor would not have been possible without the team of BiRD Lab. Many thanks to Sara and João for their help in this achievement, patience, friendship, encouragement, and generosity. I am thankful for all your support throughout this journey.

Special thanks to my family, without your support, none of this would have been possible. To my mother, for all the love, for always given me strength and encouragement. To my father, for always supporting and helping me during the most difficult times. To my twin brother, which was always by my side along this journey. I am also grateful to my grandparents, uncles, and cousins for supporting me and trying to cheer me up.

Lastly, thanks University of Minho, teachers, and staff for the warm welcome, knowledge and wisdom given during my academic journey. For making me grow not only professionally but also personally. Thank you for all these years.

STATEMENT OF INTEGRITY

I hereby declare having conducted this academic work with integrity. I confirm that I have not used plagiarism or any form of undue use of information or falsification of results along the process leading to its elaboration.

I further declare that I have fully acknowledged the Code of Ethical Conduct of the University of Minho.

Resumo

A acumulação de fadiga física resultante da execução de tarefas que obrigam à aplicação de forças intensivas durante longos períodos é um fator de risco grave para as lesões musculoesqueléticos relacionadas com o trabalho (LMERT), resultando numa debilitação e absentismo dos trabalhadores a longo prazo, perda de produtividade e piores ambientes de trabalho [1,2,3]. Tipicamente a fadiga é estimada utilizando sensores de Eletromiografia (EMG) que ainda que precisos, apresentam a desvantagem de serem intrusivos e a sua colocação necessita do conhecimento prévio da anatomia humana [4]. Uma possível abordagem é o desenvolvimento de um modelo músculo-esquelético que permita a estimação de fadiga a partir de informação cinemática. Para tal, é necessária a criação de um modelo músculo-esquelético específico ao utilizador, ajustando tanto as propriedades geométricas como as de força [5]. O dimensionamento das propriedades de força e respetivos procedimentos são em geral pouco abordados, em particular para modelos de membros superiores, pelo que esta dissertação tem como objetivo o desenvolvimento e validação de um método preciso e prático para dimensionar a força de um modelo músculo-esquelético de corpo superior. Utilizando o software open-source OpenSim, foi estudada a influência de várias abordagens de dimensionamento de força na exatidão da ativação muscular prevista pela simulação. Foram recolhidos dados experimentais de 5 participantes durante a realização de exercícios do membro superior, e posteriormente foi calculado o erro entre ativações estimadas e experimentais para cada método. Analisando os resultados, concluiu-se que os métodos de dimensionamento de força desenvolvidos não contribuíram significativamente para a diminuição do erro inicialmente calculado, no entanto verificou-se que o ajuste das propriedades de força do modelo influenciaram significativamente a precisão da estimativa quando foram aplicadas forças externas ao movimento.

Palavras-chave: LMERT; Fadiga; EMG; Modelos musculosqueléticos; Opensim.

Abstract

The accumulation of physical fatigue resulting from the execution of tasks requiring the application of intensive forces over long periods is a serious risk factor for work-related musculoskeletal disorders (WMSDs), resulting in long-term debilitation and absenteeism of workers, loss of productivity, and worse working environments [1,2,3]. Typically, fatigue is estimated using Electromyography (EMG) sensors which, although accurate, have the disadvantage of being intrusive and their placement needs prior knowledge of human anatomy [4]. One possible approach is the development of a musculoskeletal model that allows fatigue estimation from kinematic information. This requires the creation of a user-specific musculoskeletal model, adjusting both geometric and strength properties [5]. The scaling of force properties and approaches to perform such scaling are generally poorly addressed, particularly for upper limb models, so this dissertation aims to develop and validate an accurate and practical method for scaling the force of an upper body musculoskeletal model. Using the open-source software OpenSim, various force scaling approaches were investigated with respect to their influence on the accuracy of muscle activation predicted by the simulation. Experimental data was collected from 5 participants during execution of upper limb exercises, and then the error between estimated and experimental activations was calculated for each method. The results demonstrated that the developed force scaling methods did not contribute significantly to the decrease of the initially calculated error, however it was found that the adjustment of the model's force properties significantly influenced the estimation accuracy when external forces were applied to the movement.

Keywords: WMSDs; Fatigue; EMG; Musculoskeletal models; OpenSim.

Contents

List of Abbreviations and Acronyms

ATP Adenosine Triphosphate

CMC Computed Muscle Control

CNS Central Nervous System

DOF Degrees of Freedom

EMG Electromyography

H Height

iEMG Integrated Electromyography

IK Inverse Kinematics

IMU Inertial Measurement Unit

IQR Interquartile Range

M Mass

MCV Muscle fiber Conduction Velocity

MF Median Frequency

ML Mass-Length

MMG Mechanomyography

MPF Mean Power Frequency

MS Multi Variable-Single Objective

MSDs Musculoskeletal Disorders

MSK Musculoskeletal

MVC Maximum Voluntary Contraction

MUs Motor Units

NIRS Near-Infrared Spectroscopy

Pi Inorganic Phosphate

RMSE Root Mean Square Error

RRA Residual Reduction Algorithm

SS Single Variable-Single Objective

sEMG Surface Electromyography

SM Single Variable-Multi Objective

SO Static Optimization

WMSDs Work-related Musculoskeletal Disorders

Nomenclature

Hill-type musculoskeletal unit

$\boldsymbol{\alpha}$ Pennation angle

$\boldsymbol{a(t)}$ Muscle activation level

$\boldsymbol{f^l}$ Active force

$\boldsymbol{F^M}$, $\boldsymbol{F^M(t)}$ Muscle force

$\boldsymbol{f_0^M}$ Maximum isometric muscle force

$\boldsymbol{f^{PE}}$ Passive force

$\boldsymbol{f^T}$, $\boldsymbol{F^T}$ Tendon force

$\boldsymbol{f^v}$ Force-Velocity

h Pennated muscle height

$\boldsymbol{l^M}$, $\boldsymbol{l^M(t)}$ Muscle fiber length

$\boldsymbol{\tilde{l}^M}$ Normalized muscle fiber length

$\boldsymbol{l^{MT}(t)}$ Musculotendon actuator length

$\boldsymbol{l^T}$ Tendon length

$\boldsymbol{\tilde{l}^T}$ Normalized tendon length

$\boldsymbol{v^M}$, $\boldsymbol{v^M(t)}$ Muscle fiber velocity

$\boldsymbol{\tilde{v}^M}$ Normalized muscle fiber velocity

$\boldsymbol{v^{MT}(t)}$ Musculotendon actuator velocity

Mass-length, Muscle volume-based methods

$\boldsymbol{\alpha_0^M}$ Optimal Pennation angle

$\boldsymbol{\sigma_{max}^{sc}}$ Muscle specific tension

$H^{generic}$ Generic model height

H^{scaled} Subject height

$F_{max}^{generic}$ Generic maximum isometric muscle force

F_{max}^{scaled}, $f_{max}^{m,sc}$ Scaled maximum isometric muscle force

$l_{MTU}^{generic}$ Generic musculotendon length

$l_0^{m,sc}$ Optimal muscle fiber length

l_{MTU}^{scaled} Scaled musculotendon length

$M^{generic}$ Generic model total body mass

M^{scaled} Subject total body mass

$v^{m,sc}$ Scaled muscle volume

Torque based methods

σ_{max} Muscle specific tension

$a_{mech}^{g}(n)$ Estimated mechanical activation in a certain task per muscle group

c^{g} Scaling factor per muscle group

F_{max}^{m} , F_{max}^{iso} Scaled maximum isometric muscle force

M_{ergo}^{j} Experimentally measured net joint moments

$\widehat{M}_{ergo}^{j}$ Estimated net joint moments

$PSCA_m$ Muscle physiological cross-sectional area

Q_{EMG} Electromyography predicted joint torques

Q_{INV} Inverse dynamics predicted joint torques

Optimization-based methods

a_{est} Normalized estimated muscle activation

a_{exp} Normalized experimental muscle activation

$a_{est}^{mu}(t)$ Normalized estimated muscle activation per muscle over time

$a_{exp}^{mu}(t)$ Normalized experimental muscle activation per muscle over time

$F_{iso,max}^{gen}$ Generic maximum isometric muscle force

$F_{iso,max}^{scl}$ Scaled maximum isometric muscle force

mu Muscle

S Scale factor

ti Initial time

tf Final time

Force scaling methods

H Height based method

M Mass based method

ML Mass-length based method

MS Multi variable - Single objective

SM Single variable - Multi objective

SS Single variable - Single objective

Mathematical operators

∫ Integral

∑ Sum

min Minimize

List of figures

List of tables

1. Introduction

1.1. Context and Motivation

In Europe, musculoskeletal disorders (MSDs) are the most reported health problem by workers, followed by depression and anxiety. They are the second leading cause of disability in work environment worldwide, resulting in half of the costs of all diseases derived from labour [1,2,3]. The change in work style in the last two decades, in particular the adoption of remote work and the intensification of computer-dependent work, which force workers to be in the same position and execute repetitive tasks for longs periods has been contributing to the increase in these pathologies [6].

Musculoskeletal disorders (MSDs) are diseases associated with great pain, on a single or several points, that affect the normal range of motion of the body by damage in the soft tissue surrounding the joints like muscles, tendons, ligaments, nerves, and blood vessels [6]. They can be classified in MSDs of the upper limbs and neck, lower limbs and back according to the body part that they affect. Some of the most common disorders are carpal tunnel syndrome, strains, tendonitis, tension neck syndrome and mechanical back syndrome [7]. The development of Work-related MSDs (WMSDs) is related to several factors like the subject characteristics, but also biomechanical and psychosocial factors according to EU-OSHA (European Agency for Safety and Health at Work) [1,2,6]:

Biomechanical factors:

- high force application
- bad posture
- longs periods in the same position
- repetitive tasks
- exposure to vibration

Psychosocial factors:

- poor autonomy
- low motivation
- lack of support of the co-workers
- poor management of work tasks

Subject factors:

- medical record
- Physical capacity
- age
- weight
- bad health habits

The exposure to these factors, especially during long periods, contributes to accumulation of physical fatigue. As the rate of accumulation of fatigue is higher than the rate of recuperation, the balance is destroyed and enables the growth of an MSD [7]. In 2016, S. Gallagher et.al proposed MSDs as an outcome of fatigue failure process, implying that this process occurs equally in musculoskeletal tissue as in non-biological materials. Therefore, the greater the load applied, especially associated with high repetition, the lesser will be the time to tissue failure, such as muscle, tendons, ligaments, and bone [1]. The adoption of non-neutral positions while working or when executing daily activities, like twist or bend the torso, reach beyond the body, rotate, or elevate arms and hands close to maximums of their range of movement contributes to higher stress of musculoskeletal tissue, as it contracts or extends [1,8]. When works tasks are poorly managed or working conditions, the working rhythm characteristic of each subject is perturbed, moreover if is executed repetitive tasks, the body doesn´t have time to recover, resulting in fatigue accumulation that can lead to injury. [8]

Muscle fatigue assessment usually rely on electromyography (EMG) sensors, which are highly influenced by electrode placement, signal noise and physiological factors that may lead to inaccurate measures [4], in addition to the need for knowledge in anatomy and a thorough skin preparation by the user, which makes it

impractical. Thus, it is necessary to develop a system capable of accurately estimate muscle fatigue without harm to the body, and thus prevent the formation of MSDs. Musculoskeletal models are computational models that recreate human musculoskeletal system, allowing the simulation of human body motion and estimation of muscle internal loads and joint reactions that otherwise are difficult to measure experimentally [9]. Given that the onset of muscle fatigue is manifested by a reduction in muscle strength and adaptation of body posture, these models can be an alternative to conventional EMG fatigue detection methods [4,10]. The scaling of the musculoskeletal model is a fundamental step to perform before starting the simulation, with high influence on the accuracy of the quantities to be estimated. This process consists of adjusting model properties to subject characteristics, as faithfully as possible, being these length, mass, or force parameters. Musculoskeletal modeling and simulation software, such as OpenSim, possess tools that allow the scaling of mass and length proprieties of the model, however, do not address force fitting.

1.2. Objectives

Although, there are several studies and approaches concerning the scaling of model´s musculotendon length proprieties and geometry, the scaling of muscle strength or force capacities and its impact is not as addressed, especially those involving upper body models. Thus, aiming for a highly subject-specific model with further application on muscle fatigue assessment, the main goal of this thesis is the development and validation of an accurate and practical method to scale the strength of an upper body musculoskeletal model. To achieve this end, the following objectives must be accomplished:

- Conduct a review of the available literature regarding the approaches used to perform force scaling on upper body musculoskeletal models.
- Create or adapt an upper body musculoskeletal model according to the requirements of the study.

- Develop a method capable of scaling the force proprieties of model based on kinematic data and open-source software.
- Validate the developed approach by collecting experimental data.

2. Theorical fundamentals

2.1. Skeletal muscle

In human body there are three types of muscle: cardiac, smooth and skeletal. The first two types are of involuntary control, where the first is responsible for the contractions in the heart that allow the pumping of blood into the body, and the second is found in organs such as the intestine and stomach, where it promotes slow contractions. Finally, the skeletal muscles are connected in its extension to bones by means of tendons and are responsible for body posture, generation of movements and force according to one's own will [11]. In this work we will focus only on this type of muscle.

2.1.1. Muscle structure and contraction

Skeletal muscles are the human body actuators, responsible for generating force and movement capable of sustaining body posture and perform innumerable tasks of daily life. They are constituted by clusters of basic units of fibers (Figure 1), also known as myofibers or muscle cells, surrounded by connective tissue and connected to motor neurons, the association of the last with a fiber is called motor unit. Each fiber in turn results from an agglomerate of myofibrils made up of myofilaments, mostly actin and myosin proteins. The combination of this proteins

attached by cross-bridges forms the muscle generators units of force and power know as sarcomeres [12,13].

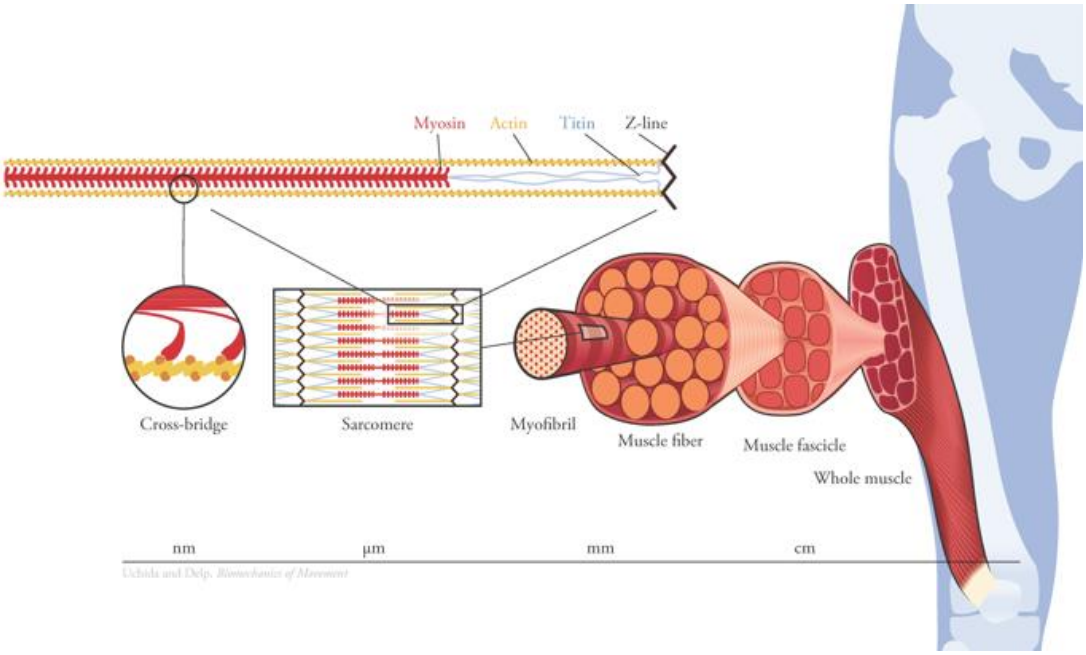

Figure 1 - Muscle structure. Adapted from [14].

The sliding filament theory is the most accepted conjecture to explain the process of muscle contraction, which consists in sliding of actin over myosin filaments. When the neural signal transmitted as electrical impulses from CNS (Central Nervous System) to motor neurons reaches the muscle fiber, the calcium (Ca^{2+}) stored on sarcoplasmic reticulum is released to the cell cytoplasm, binding myosin to actin and forming a new cross bridge, meditated by ATP (Adenosine Triphosphate) hydrolysis. Resulting in shortening of sarcomere and so force generation, transmitted along the entire muscle, tendon and finally joint. This cycle is repeated by cross-bridge wrecking when ATP molecules binds to myosin again, and cross-bridge formation occurs again until neural excitation stops. Ceasing the neural stimulus, Ca^{2+} ions return to sarcoplasmic reticulum and the muscle returns to its initial state of relaxation [12].

Muscle contractions can be classified as static or isometric, dynamic concentric or isotonic concentric, and dynamic eccentric or isotonic eccentric, depending on the movement effected by the muscle to develop force. These types of contractions are present on daily life actions, like lifting an object (Figure 2). Initially, the dumbbell is

held by a force generated by the muscle while maintaining the same position of the limbs and joint, this called an isometric contraction (Figure 2(a)), resulting in a force with lower module. For example, when lifting the dumbbell, the force is exerted while bending the arm, there is joint movement and muscle shortening, representing an isotonic concentric contraction (Figure 2(b)). Finally, when putting the dumbbell down (Figure 2(c)), occurs stretching of the muscle and extension of the arm, this is referred as an isotonic eccentric contraction [4,12].

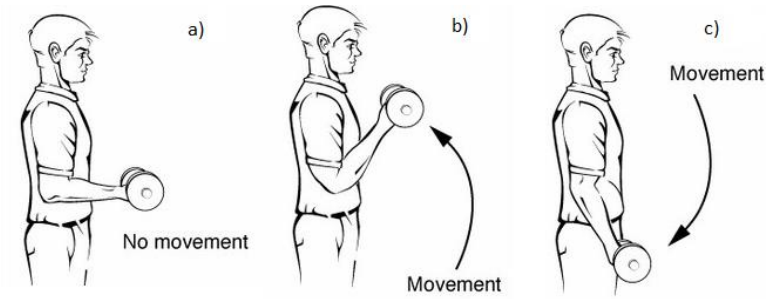

Figure 2 - Lifting a box. a) isometric contraction; b) isotonic concentric contraction; c) isotonic eccentric contraction. Adapted from [15].

2.1.2. Muscle force and fatigue

One of the factors that influence the mechanical function of the muscle is the arrangement of the fibers. Depending on the muscle type, muscle fibers can be orientated in parallel or form an angle relative to muscle line of action, known as pennation angle, promoting an increase in muscle force since more fibers are concentrated in the same muscle volume. The muscles with this configuration are called pennate muscle and are the most common type on human limbs. During contraction of the muscle, the pennation angle increases, contributing to change on muscle shape by shortening its length and extending its thickness and width (Figure 3) [12,13].

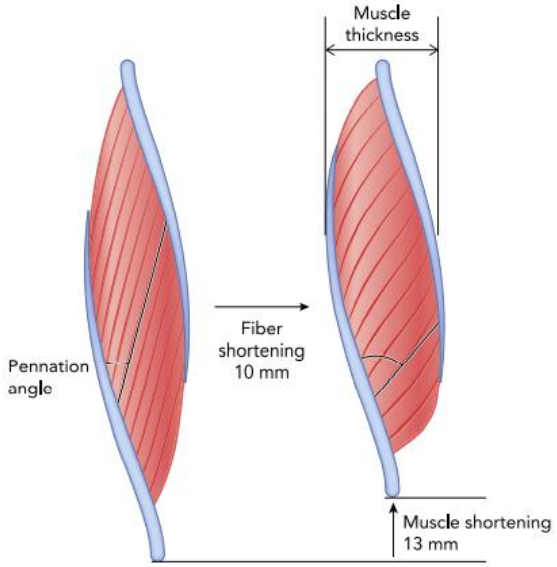

Figure 3 - Muscle and fiber shortening. Adapted from [13].

The force generation capacity is dependent on initial fiber orientation and the change in thickness during muscle contraction, as the ratio of fiber length to muscle length increases due to muscle shortening, the force transmitted to the joint decreases [12]. The velocity of contraction is correlated with myosin attachment to actin by ATP hydrolysis, influencing force. Faster concentric contractions result in lower muscle strength, contrary to the increased force output in eccentric contractions performed under the same conditions. Thus, maximal force is produced for an optimal length, pennation angle and velocity, involving an optimal overlap of myofilaments contributing to greater cross-bridge formation. Other factors that may influence muscle force are neural excitation, stimulation frequency, fiber type and calcium ions concertation on sarcoplasmic reticule [12,16].

Muscle fatigue can be seen as a combination of failures of key physiological systems at the level of nerve stimulation, energy, and oxygenation. The origin of muscle fatigue can be attributed to changes in motor pathway, involving peripheral fatigue associated to the neuromuscular junction (junction between neuromotor and muscle fiber) and central fatigue on the CNS. During the execution of high muscle effort tasks, the excitation input inferred by the CNS and excitability of motor neurons decreases (central fatigue), this occurs to protect the muscles from severe damage, reducing the rate of action potential fired by motor neurons that reach muscle fibers.

This leads to an increase in Pi (inorganic phosphate) molecules that causes less uptake of calcium ions to sarcolemma (peripheral fatigue), interfering with cross-bridges formation and so decrease in force, that is a signal of muscular fatigue. The decreased oxygen supply to the muscle due to obstructed blood circulation during exercise is also a factor that can lead to muscle fatigue, as the ATP demand cannot be met [4,17].

From a biomechanical view, muscle fatigue can be defined as a diminution in capacity of generating force during muscle contraction and is associated to a decrease of maximum voluntary contraction (MVC) force. The number of cycles and effort applied that is necessary to reach muscle fatigue level differs from person to person, with characteristics like gender, age, and muscle proprieties, thus is difficult to define a floor in detection of fatigue [4,17].

2.2. Measurement of fatigue

Usually, the evaluation of fatigue is conducted via Electromyography (EMG) techniques, that corresponds to the record of the muscle electrical activity in response to a force exertion task [17]. The most common EMG techniques to detect fatigue is sEMG (Surface Electromyography) because it is less invasive, as the electrodes measuring the electrical potential are placed only on the surface of the skin.

The presence of fatigue on muscle is translated by changes on EMG signal amplitude and frequency parameters, usually obtained by means of signal processing methods, on time and frequency, respectively. These changes can be attributed to an increase in motor unit recruitment and firing rate in order to maintain force when muscle reaches fatigue. It is also traduced by a decrease in muscle fiber conduction velocity (MCV) due to accumulation of lactate acid, produced in anaerobic conditions, as form to protect organism damage [4]. The comparison between time and frequency analyses can be seen in Table 1.

Table 1 - sEMG time and frequency analyses

	sEMG - time domain
Principle	Increase in amplitude of EMG signal with fatigue due to greater recruitment of MUs (Motor Units) in dynamic contractions [4]
Parameters	Root Mean Square (RMS); Integrated Electromyography (iEMG) [4]
Strengths	Measure of force magnitude [18]
Limitations	Not very accurate, better associated with spectral methods; Subject specific fatigue threshold [4]
	sEMG - frequency domain
Principle	EMG spectrum frequencies decrease when muscle is fatigued. The current value of parameter is compared with the value of a state without fatigue and registered the differences [4]
Parameters	Mean power frequency (MPF); Median frequency (MF); Muscle fiber conduction velocity (MCV) [4]
Strengths	More reliable and most used in isotonic contractions [4]
Limitations	Subject specific fatigue threshold [4]

Amplitude based measurement of fatigue is less used due to the instability of its behaviour, since it can increase, decrease or suffer no change. It´s highly dependent on muscle type and intensity of contraction. On other hand, the frequency parameters have the same relation of decreasing regardless of fatiguing conditions [4,19,20]. Overall, sEMG has many limitations in respect to high sensibility to electrical noise, electrodes placement and area, conductive gel used between skin and electrode, muscle contraction intensity and blood flow, and many others. Its use in isotonic contractions is questionable, as it can be influenced by physiological factors such as muscle length and joint movement changes [4]. In addition to its impracticality of use, which requires the rigorous placement of multiple sensors, and an exhaustive preparation of the skin that can be uncomfortable for the user.

Other methods beyond EMG to evaluate fatigue are NIRS (near-infrared spectroscopy), infrared thermography and MMG (Mechanomyography), described in subsequent table.

Table 2 - NIRS, infrared thermography and MMG evaluation methods

	NIRS (near-infrared spectroscopy)
Principle	During execution of effort, the body necessity for oxygen is greater, contributing to an increase in oxygenated hemoglobin. The difference between oxygenated and deoxygenated hemoglobin in blood is proposed as an indicator of muscle fatigue, measured using near-infrared radiation ray and optical sensors [4,21]
Conclusions	Muramatsu et al. (2013), found that this difference is constant when muscle isn´t in fatigue conditions and that it increases with fatigue as time pass [20]
Strengths	Non-invasive; The relation is not dependent on load; Can be used on isometric and isotonic contractions; Give information about fatigue progression velocity; Complement sEMG [4,21]
Limitations	The blood oxygenation is influenced by subject characteristics and breathing; Affected by skin fatness and melanin concentration [21,22]
	Infrared thermography
Principle	While exercising there is generation of heat due to metabolic process, increasing temperature around the contracted muscle. This difference in skin temperature can be evaluated by infrared thermography [23]
Conclusions	Bartuzi et al. (2016) studied the correlation between muscle fatigue and temperature measured by infrared thermography when compared with EMG on low load isometric contraction of upper limb. They conclude that muscle temperature increases with higher muscle contraction forces, where fatigue is greater. It has a great

	correlation with the analysed EMG frequency parameters [23]. Hadžic et al. also obtained same conclusions when doing trials with concentric contractions of lower limb, though it is needed more research [24]
Strengths	Non-invasive; Contactless; Good sensitivity for low muscle load [23]
Limitations	More study is needed for non-athletes and elderly population; Influenced by variations in temperature and skin fat [23,24]
	MMG (Mechanomyography)
Principle	Records the muscle vibrations arising by motor unit activation. The same parameters for sEMG, amplitude and frequency, are used [4]
Conclusions	Tarata et al. (2003), compared MMG And EMG signals regarding fatigue monitoring. They found that RMS and MF parameters of MMG increased and decreased in response to muscle fatigue on sustained contractions, presenting the same relation as sEMG [25]
Strengths	Detects difference in neural activation; not affected by electromagnetic radiation; less variability between genders [4,25]
Limitations	Use in dynamic contractions is limited; Crosstalk contamination [4]

The NIRS and infrared thermography are non-invasive methods that can be used evaluate fatigue however is still necessary more studies to prove it´s efficacy and not only as EMG complement. MMG can also reveal central and peripheral fatigue as EMG, it isn´t affected by electromagnetic radiation and can be used in individuals with chronical electric implants unlike EMG. However, there is no standard protocols for signal acquisition like in EMG systems, and the MMG signal from the muscle to be measured can be disturbed by the activity of the neighbouring muscle, known as crosstalk contamination [4,25,26].

Besides the methods stated above, it is also possible to infer fatigue trough biomarkers like ATP metabolism, Oxidative stress and inflammatory markers [17].

2.3. Musculoskeletal models

The development of musculoskeletal models enabled the estimation of internal loads of muscles, ligaments and joint reactions that are difficult measure by experimental tests, and so allow to identify the source of abnormal movement in patients with neuromuscular or musculoskeletal disorders and define better recovery strategies. These models are constituted by rigid bodies or segments, that normally represent bones, and joints that connect them and stimulate their movement through forces generated by enveloping muscles [27,28]. Musculoskeletal systems simulations are dependent on formulation of musculotendon dynamics, that can be defined by Hill-type musculotendon models, which are used on simulation frameworks like Opensim. In Hill-type models musculotendon units (Figure 4) are defined as extensible strings connected to bones, in which muscles fibers are assumed as being homogenous, keeping the same height and area as the angle between tendon and fiber, the pennation angle, is commuted [29].

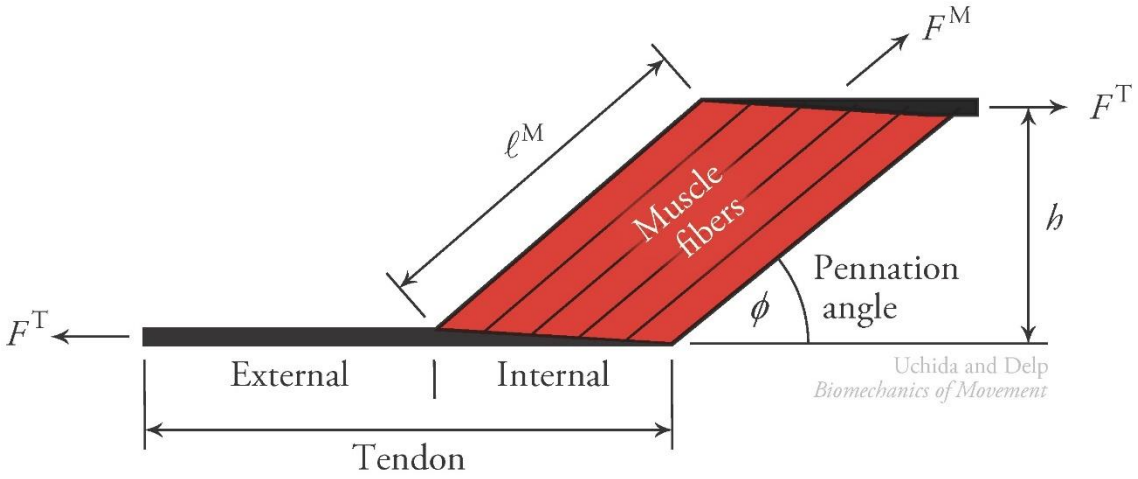

Figure 4 - Geometric representation of musculotendon unit. Where ϕ-pennation angle; h-pennated muscle height; l^{M}- length of muscle; F^{T}- Tendon force; F^{M}-Muscle force. Adapted from [14].

The muscle force is computed based on a combination of activation and contraction dynamics (Figure 5), where the last uses the results from activation dynamics, musculotendon length and velocity to compute muscle length, velocity, and force [29].

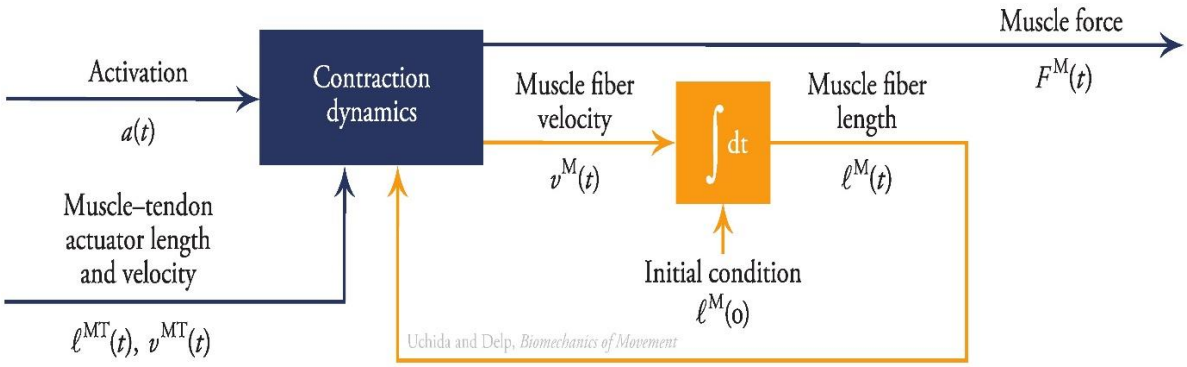

Figure 5 - Schematic representation of musculotendon dynamics. Adapted from [14].

The activation dynamics represents the relation between neural excitation and muscle activation level (a(t)), that can increase or decrease dependent on the availability of calcium ions. On the other hand, contraction dynamics defines the relation between muscle activation and musculotendon force on Hill-type models. The Hill-type model is defined, as seen in Figure 6, by an elastic tendon (3) with length l^T, forming a pennation angle (α) with muscle fiber of length l^M. This fiber is constituted by two parallel components, an active contractile component (1) and a passive elastic one (2) [29,30,31].

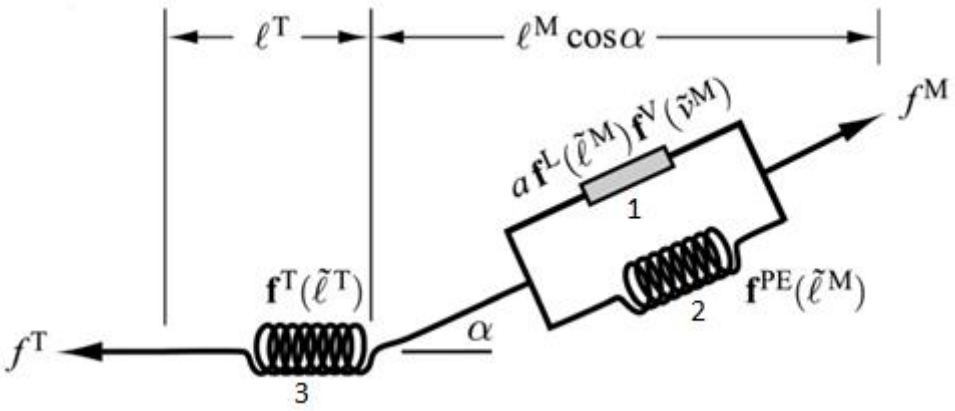

Figure 6 - Hill-type musculotendon unit. Adapted from [29].

This model assumes that muscle force is only dependent on muscle activation (a), length and velocity. The dependence of these elements' forces with tendon length (l^T), muscle length (l^M) and velocity (v^M) can be described by the following curves.

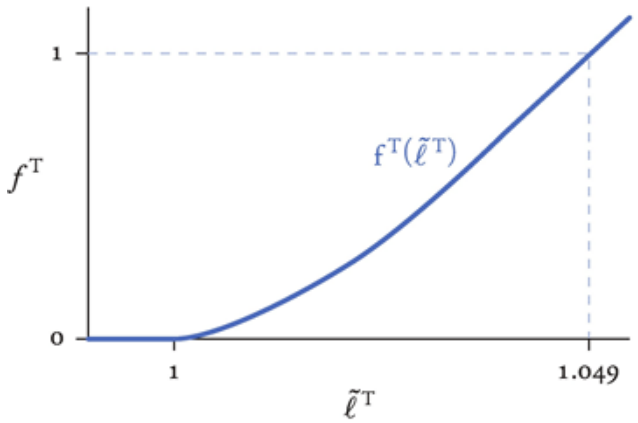

Figure 7 - Tendon-Force length curve ($f^T(\tilde{l}^T)$). Adapted from [14].

The tendon-force length curve (Figure 7) represents the change of tendon force (f^T) with the tendon length ($\tilde{l}^T$). Behind the tendon slack length this force is null, however as tendon stretches beyond this length a force is produced and increases exponentially with tendon strain [29].

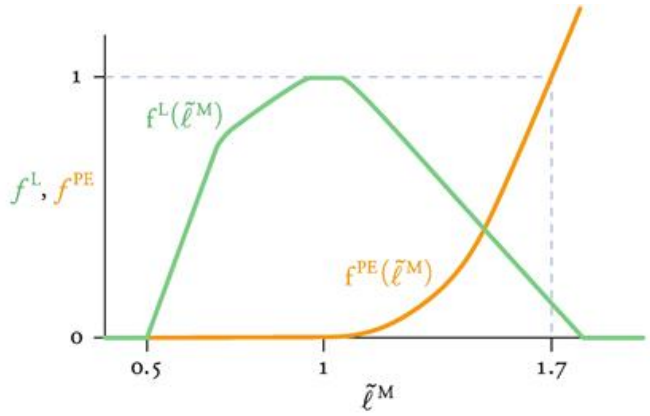

Figure 8-Active force–length curve (green) ($f^l(\tilde{l}^M)$) and passive force–length curve (orange) ($f^{PE}(\tilde{l}^M)$). Adapted from [14].

When the muscle is activated, an active force (f^l) defined by a gaussian function is generated (Figure 8, green curve), and it´s value is higher or lower depending on muscle length ($\tilde{l}^M$), being maximal at optimal muscle length. On the other side, when the muscle is stretched beyond a threshold length, a passive force (f^{PE}) is developed and growths exponentially (Figure 8, orange curve) [12,29].

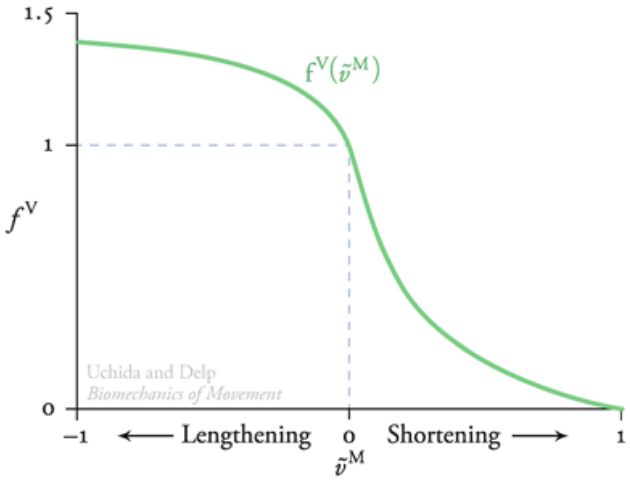

Figure 9 - Force–Velocity curve ($f^V(\tilde{v}^M)$). Adapted from [14].

When executing concentric contractions, which involves the shortening of the muscle, the force produced is greater for lower velocities ($\tilde{v}^M$). On the other hand, movements that contribute to muscle lengthening are characterized by a higher strength when executed faster [12,29,31].

All these curves can be related by equation (1), where the muscle force is in equilibrium with tendon force, without considering the effect of muscle mass and rigidity of tendon. Where f_0^M is the maximum isometric muscle force when muscle is in its optimal length, and the parameters with tile, $\tilde{l}^M$, $\tilde{v}^M$ and $\tilde{l}^T$ are normalized by muscle fiber optimal length, maximum muscle contraction velocity and tendon slack length, respectively. This formulation is considered as the condition of initialization of the simulation process, which has many solutions [29].

$$f_0^M \left(a f^L\left(\tilde{l}^M\right) f^V\left(\tilde{v}^M\right) + f^V\left(\tilde{v}^M\right) + f^{PE}\left(\tilde{l}^M\right)\right) cos\,\alpha - f_0^M f^T\left(\tilde{l}^T\right) = 0 \quad (1)$$

To obtain a single solution, the next step involves the calculation of normalized muscle velocity ($\tilde{v}^M$) by equation (2), that is constrained by a maximum pennation angle value and a minimum muscle length value in order to have a better approach to muscle natural physiology [27].

$$\tilde{v}^M = f_{inv}^V \quad \left(\frac{f^T(\tilde{l}^T)/\cos\alpha - f^{PE}(\tilde{l}^M)}{a\, f^L(\tilde{l}^M)}\right) \qquad (2)$$

Thus, the force generated by Hill-type musculotendon models is computed based on the constant parameters of muscle and tendon proprieties, namely muscle fiber optimal length, maximal muscle contraction velocity, tendon slack length, maximal isometric muscle force and optimal pennation angle, that are usually obtained by cadaveric studies [30].

3. Required utilities

3.1. OpenSim

OpenSim is an open-source software that enables the creation and sharing of musculoskeletal models and dynamics simulations of movement by the user, allowing the study of the influence of neuromuscular system on forces and joints moments produced by muscles. The analyses and studies effectuated by these simulations help to understand the biomechanics of movements, making it possible to improve knowledge about physical disabilities and to develop more effective recovery strategies [28,32].

In OpenSim models the bones are defined as rigid segments, in which the child segment moves relative to a parent segment by means of a joint. All segments have a parent except for the ground, and the range of motion of the joint can be constrained by limits. Muscles, based on Hill-type models, wrap to these segments trough insertion and origin points, creating a path representing the muscle´s line of action. The force produced by these actuators is dependent on its path, fiber and tendon length, the rate of change of length and activation level. In addition to the active forces from muscles or actuators, external forces obtained experimentally by force plates, such as ground reaction forces, or internal passive forces from springs or dampers can also be applied to the model. And lastly, model´s controllers generate and regulate muscle excitations. In sum, OpenSim models, are defined by bodies, joints, forces, constraints, and controllers, whether these are lower (Figure 10), upper extremity, head, neck, human or animal models [32,33].

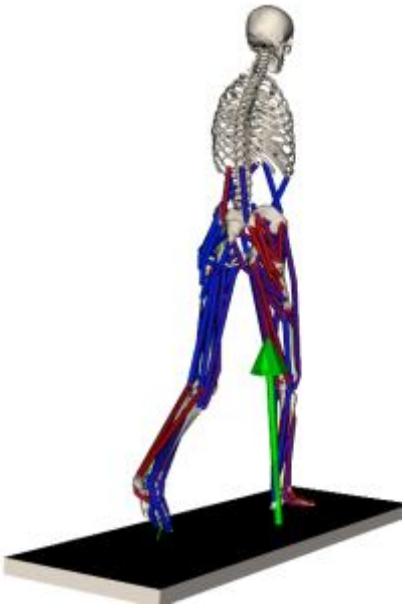

Figure 10 - Lower extremity model on OpenSim, with muscles and ground forces applied. Adapted from [32].

Depending on the application and data availability of the study, model´s controls or response can be found trough inverse or forward simulations methods. Inverse methods like inverse dynamics (IK), static optimization (SO), and computed muscle control (CMC), start from marker trajectories positions, force data and

velocities that describe a specific motion and determine joint and muscle kinetics, and musculotendon dynamics responsible for generating that movement, as described by the red arrows on Figure 11 [32,34].

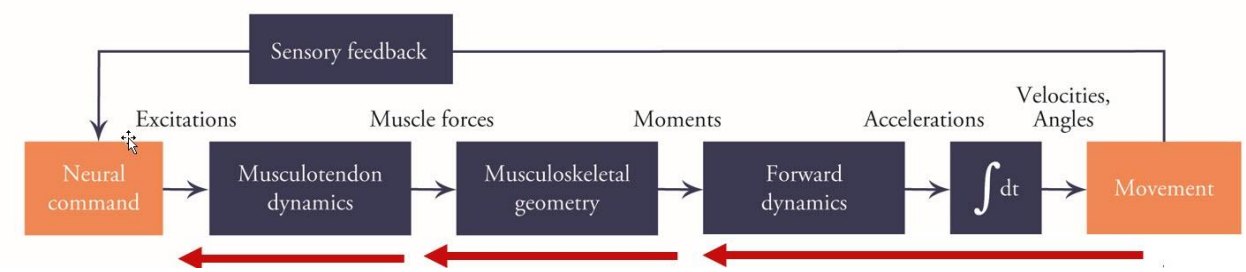

Figure 11 - Inverse method. Adapted from [34].

On the opposite, forward methods like forward dynamics tool follow the blue arrows of Figure 11, driving the movement of a model departing from estimated muscle excitations, joint torques, applied forces or other controllers [32,34].

3.2. Xsens MVN

The Xsens MVN is a motion capture system based on inertial measurement units (IMUs) sensors. It can be used indoors and outdoors and capture several types of motions, it has been applied on diverse fields like biomechanical, rehabilitation, sport,3D animations and virtual reality [35,36].

The segments position and orientation are computed in real time by accelerometers and gyroscopes included on the 17 inertial and magnetic measurement units trackers placed on the subject that executes the motion. The orientations are registered and visualized on a biomechanical model calibrated with user body segment dimensions [36].

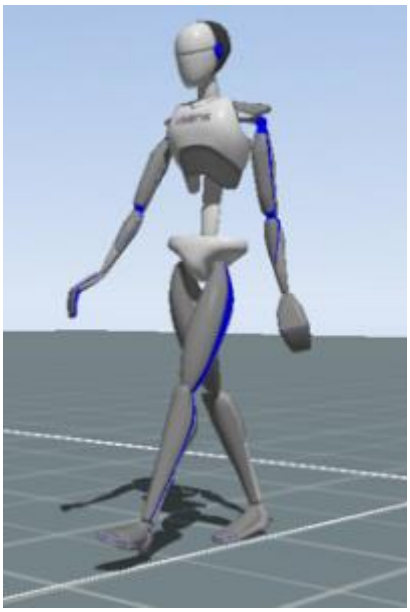

Figure 12 - Xsens MVN body model. Adapted from [35].

This model is formed by 23 rigid body segments attached by 22 joints, each with 3 degrees of freedom (DOF) . The definition of segments axes and frame origin is based on ISB (International Society of Biomechanics) recommendations [37]. The kinematic data of the motion described can be exported in several files format: BVH, FBX, C3D, MVNX, being the last two the most useful for this work. The C3D format contains information about the anatomical bony landmarks' positions during motion, registered as markers on the Xsens MVN body model and represented on Figure 13 by the points designated with "p" letter. While the MVNX contains segments' position, angular velocity, acceleration, orientations in quaternions and joint angles in ZXY and XZY Euler angle sequence, that may be used as input of human body simulations [35].

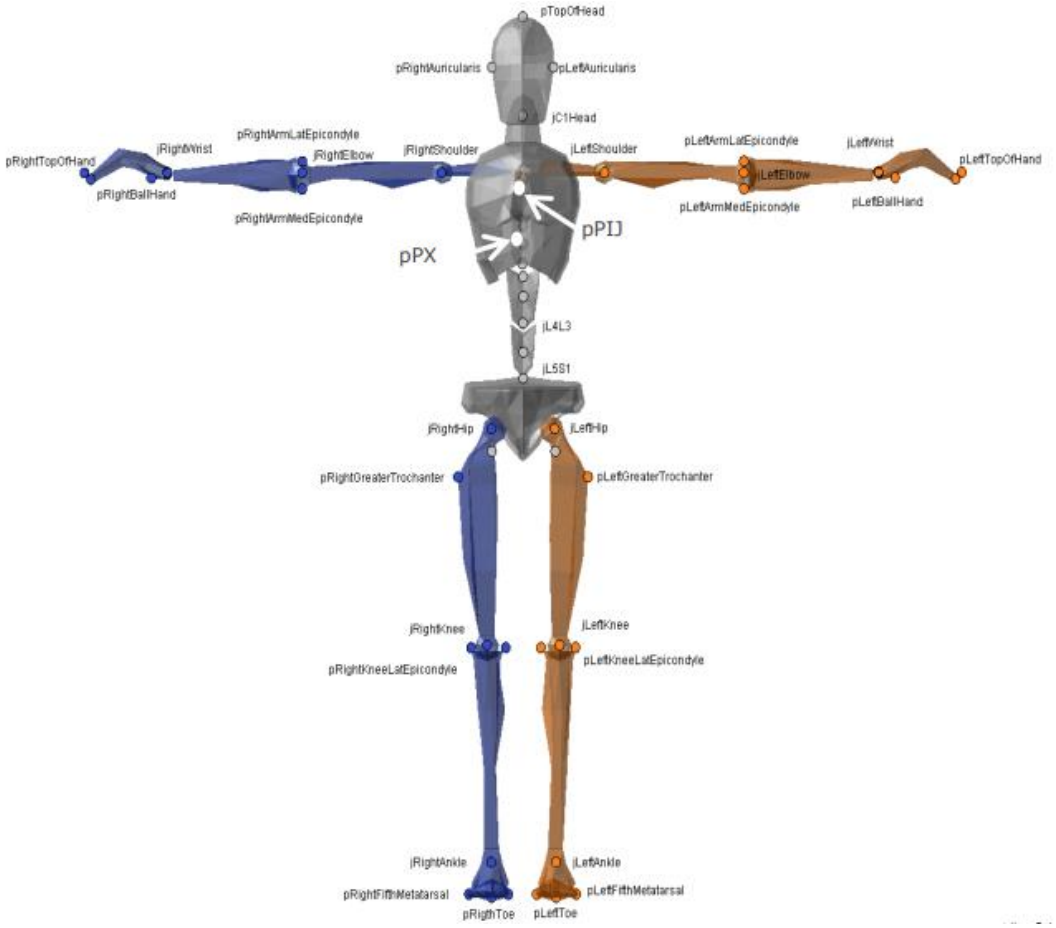

Figure 13 - Markers of Xsens exported on C3D.Adapted from [35].

Magnetic interferences of the surrounding environment, sensor noise and displacement of the IMUs related to soft tissue, are the main factors that affect motion tracking accuracy [35,36]. In 2018, Michael Sweet et al., analyzed the effect of IMUs (Xsens MTw Awinda) displacement on knee angle variability during gait. Though the study sample was small, the results demonstrated that initial IMU placement can lead to a variance of 5-10 degrees in the measured knee angle value [38]. Richard Hsiao et al. (2017), studied the effect of velocity on Xsens IMUs tracking accuracy by collecting data at 40 bpm, 80 bpm and 120 bpm while performing neck flexion. The ground truth of the movement was extracted with the aid of a high-speed motion capture camera. The results indicated a decrease in precision of IMUs motion capture system with the increase of the movement speed [39].

3.3. Upper body model

The model used in this project is defined only by bodies on upper body, since the main interest is the study of the upper arm dynamics. For that purpose, it was selected the combination of two models already developed, the arms of "Upper extremity model" developed by Holzbaur et al. [40] and the body of "Thoracolumbar Spine and Rib Cage model" by Bruno et al. [41] (Figure 14).

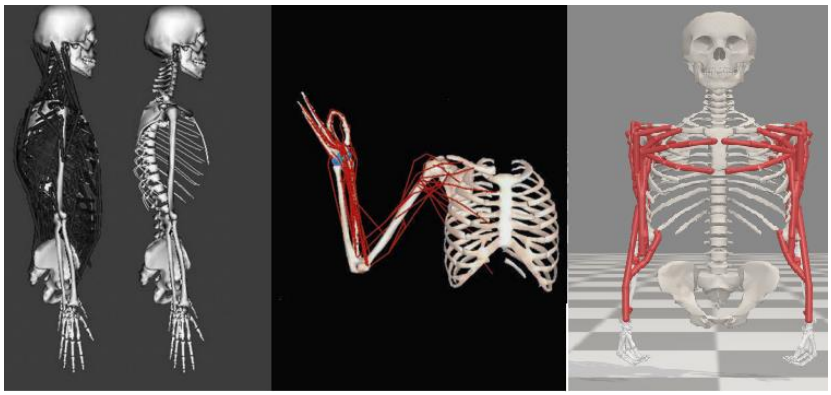

Figure 14 - Thoracolumbar Spine and Rib Cage model (left); Upper extremity model (center); model used in this project (right). Adapted from [40,41].

The thorax in "Thoracolumbar Spine and Rib Cage model" (Figure 14 (left)) is represented by twelve ribs on each side, each one with mobility of one DOF, connected to spinal column vertebra. The sternum is connected to clavicula and scapula, and has tree rotations on x, y, z axis. The head and neck are modelled as a single body and a have tree DOF as well as pelvis, column´s vertebrae, and abdomen [41]. The arm in "Upper extremity model" (Figure 14 (center)) is constituted by humerus, radius, ulna, and hand, linked by two joints. The shoulder joint that links humerus to scapula enables the movements of abduction/adduction in y-z plane, flexion-extension in x-y plane and internal/external rotation in z-x plane in OpenSim coordinate system. On the other hand, elbow and wrist joint has 2 DOF, flexion-extension and internal/external rotation [40]. To each body on the two models, a muscle is associated with a with a particular path point. In accordance with our study purpose and hardware limitations, some changes were made to simplify the model

regarding muscle composition and joint motion definitions. In the lower arm, extensors and flexors muscles of the hand were removed and the wrist joint was deprived of motion, as well as the rib, column, neck and sternum joints. Abdomen and respective muscles were removed from the model, as its movements were not considered as a study factor in this work.

Resulting on final model (Figure 14 (right)) with 46 muscle actuators and sixteen joint coordinates: shoulder joint with 3 DOF and elbow joint with 2 DOF for each arm, and pelvis joint with 3 DOF in rotational and 3 DOF in translation.

3.4. OpenSim MOCO

Moco ("musculoskeletal optimal control") is an OpenSim extension capable of solving several problems related to biomechanics, such as motion tracking, motion prediction, parameter optimization, model fitting or electromyography-driven simulation. This open-source and customizable software package can predict a trajectory usually quicker than the others by using direct collocation method and accepts almost any Opensim model [42]. The optimal control problem is formulated by providing a model, goals, and constraints, defined by the user or retired from Moco library. Additionally, it can be given reference data (markers coordinates, external forces and muscle activity) to track while predicting a motion or optimizing parameters. The study, *MocoStudy*, starts by describing the problem with *MocoProblem* class by setting the cost function (time, states, kinematic constraints, controls…), the model and controls to which it is subjected, with respect to bounds like time, states, controls, or model properties to optimize (Figure 15). After establishment of the problem, *MocoSolver* class is called to solve it and find the optimal solution, while satisfying the kinematics constraints. *MocoSolver* supports both forward and inverse dynamics, and enables the setting of convergence tolerance, constraint tolerance and number of mesh intervals of the problem [42].

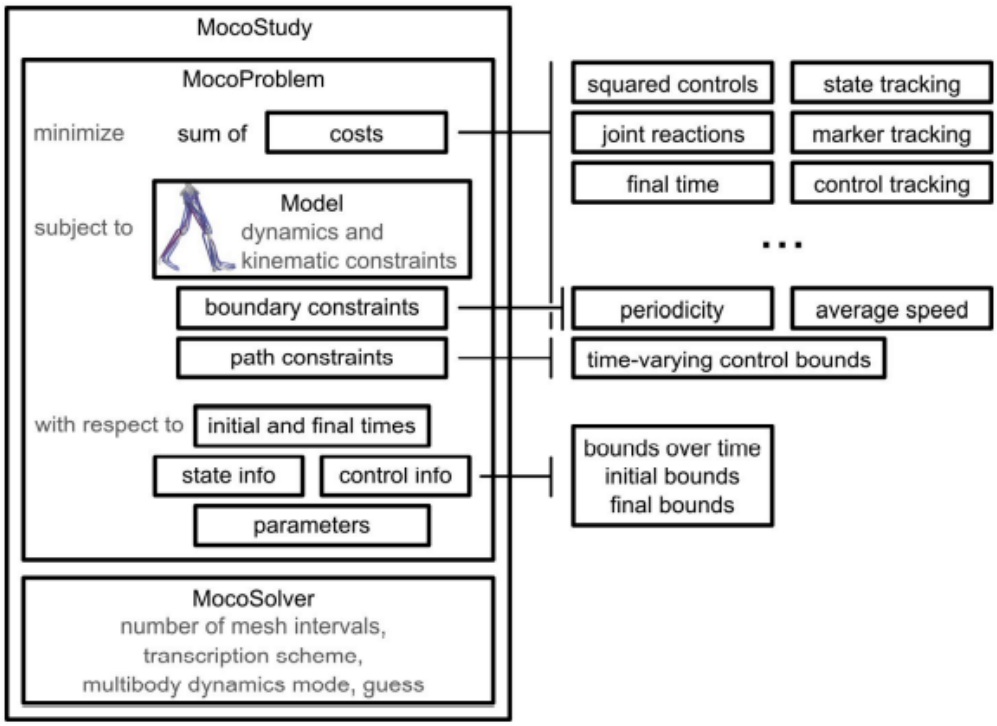

Figure 15 - Synthesis of *MocoStudy*. Adapted from [42].

Depending on the problem the motion can be prescribed, tracked, or predicted. Moco library possess tools that enables the resolution of problems dependent on the motion observed, namely *MocoInverse*, that from the prescribed movement solves muscle/actuator redundancy problems, whereas *MocoTrack* enables motion tracking. In both tools, there are model's constraints and motion data (coordinates, marker trajectories or external loads) are provided, however the way how the motion is handled while computing the controls and actuators states is different. While in *MocoInverse* the problem is subject to the prescribed motion, beyond the constraints defined, following it strictly while minimizing the costs, in *MocoTrack* deviations from the kinematic provided are predicted while obeying to kinematics constraints, obtaining a solution that minimizes the error between reference data and the data predicted, in addition to other costs. Regarding the prediction of muscle activity, both tools when applied the same model and kinematic data, showed for most muscles a peak muscle activity timing similar to the measured EMG data from a gait cycle, as well as resemblances with Opensim SO and CMC results [42].

MocoInverse is a faster and more robust option if the motion is known and must be closely followed, *MocoTrack* is more suitable when the goal is to study deviations from the original data. For other problems not standardized, like motion prediction, it is necessary to develop a specified study [42].

4. Literature review

4.1. OpenSim uncertainty

Computational models and simulation software allow to recreate, to a certain extent, human musculoskeletal system and from there draw results and conclusions, that are difficult to obtain otherwise. However, it is crucial to verify their conformity with reality, and characterize its error and uncertainty.

In order to understand OpenSim software error and it´s variables, an advanced search was executed in Scopus and PubMed databases with keywords “OpenSim”, “error”, using Boolean operator “AND”. Most results were common to both databases and mainly focused its analysis on gait and lower-limb models. Only studies that quantified Opensim's error and assessed the causes of its variation were selected. Applying this criteria, five studies were examined, whose main conclusions are described below.

4.1.1. Results

In 2014, Beth Lewandowski et al. using an Opensim full body model with muscle type Thelen 2003 determined OpenSim calculation error by comparing the difference between estimated and experimental ankle torque, obtained through

isometric and isokinetic contractions tests. They reported a maximum difference of 3.3 % for isometric measures and 4.8 % for isokinetic analyses [43]. Ursula Trinler et al. (2018), characterized the error between experimentally obtained EMG and the lower limb muscle activations estimated by OpenSim's Static Optimization (SO) and Computed Muscle Control (CMC), in addition to its variability with subject walking speed. The OpenSim generic model gait2392 was scaled for each of ten individuals. The joint angles were determined by inverse kinematics and subsequently muscle activation by SO and CMC. Comparing them to the experimental muscle activation obtained from the EMG, the mean absolute error ranged from 15 % to 68 % for SO, and from 13 % to 69 % for CMC, being lower for slower walking speeds [44].

Different modelling approaches and definitions like joint axes orientations, DOFs, geometry, muscle parameters, number of muscles or segments and mass proprieties can interfere on the calculation of joint kinematics and further joint moments, which will consequently induce changes on predicted muscles' force and activation [45,46].

In 2015, Casey A. Myers et al. accessed through probabilistic methods, the uncertainty propagation on consecutive stages of a gait simulation. Files with variations of model initial proprieties (mass, inertia, maximum isometric force, tendon slack length) and markers positions were introduced as input of OpenSim inverse kinematics, inverse dynamics and static optimization tools and used to generate sequential outputs of joint kinematics, moments, and muscle forces. The 5 % and 95 % confidence bounds were calculated for each of these metrics. The results demonstrated that the combined effect of all sources of uncertainty in simulation inputs had significant impact on outputs, with mean confidence bounds that ranged from 2.7° to 6.4° in joint kinematics, 2.7 N to 8.1 N m in joint moments, and 35.8 N to 130.8 N in muscle forces. The authors pointed out that uncertainty associated to marker movement artifact and placement error had a major impact on joint kinematics and joint moments, while changes in muscle parameters strongly influenced muscle forces, and in turn joint moments were sensitive to body segment variations. Additionally, output sensibility was dependent on gait portion analyzed [47]. Sarah A. Roelker et al. (2017) investigated the difference between the outputs computed using

Opensim IK, RRA (Residual Reduction Algorithm) and SO of four musculoskeletal models, anthropometric scaled to the same subjects and with the same input data. The four models were distinct between each other, carrying different muscle parameters like maximum isometric force, coordinate system, number of body segments and DOFs. Significant differences were found between models on joint angles magnitude determined by inverse kinematics, because of disparities in definitions of pelvis neutral position and knee joint center, which contributed also to joint moments variations. In addition to influence of joint kinematics, the unequal peak isometric force values also contribute to variation amid models on peak muscle force and peak activation magnitude by a maximum of 151 % and 1500 %, apart from greater or lesser RMS error between experimental EMG and estimated muscle activation [46].

Besides model's proprieties, the scaling process of a generic model to specific user conducted primary, may have impact on simulated joint kinematics and kinetics. The position of the model's markers and the dimensions of each body relative to the subject's real measures strongly influence the simulation output. Thomas K. Uchida et al. (2022), studied the influence of this uncertainty on OpenSim inverse dynamics calculation of joint angles, moments and power on gait models, revealing that a difference of only 2 cm between model´s and physical markers position can cause the estimated peak joint angle to vary up to 15.9°, moment to 26.6 Nm, and power by 75.9 W [48].

As described, there is always an error associated to estimated quantities from simulations, that can be larger or smaller depending on the modeling variables and input parameters, thus whenever possible the predicted results should be validated against experimental measures and/or published studies, while also having special attention to error aroused from input data collected, like EMG, markers positions and joint angles from Mocap systems.

4.2. User specific scaling

One of the ways to minimize this error is by adjusting the model as close as possible to the individual user characteristics. Ideally, the musculoskeletal model

should be built based on the individual's own bone and muscle structure, resulting in a highly subject-specific model, but this is a time-consuming and costly process, so generic models with basis on cadaveric studies are usually chosen. Models known as scaled-generic, result from the adaptation of parameters from a generic model to a particular individual [49]. Contrary to subject-specific models that are built on user real geometry and muscle data derived from medical imaging, in scaled-generic models the generic body segments, joint orientations, and muscle architecture are adjusted to user by means of scale factors computed from markers coordinates, determined via optical trackers or IMUs systems [50].

In 2020, James P. Charles et al. assessed the accuracy of muscle torques obtained by lower limb models with individualised properties and models built using generic values from younger and older population. Muscle torques estimated by models derived from MRI were closer to the experimental values than those predicted by the generic models, where in the latter the rmse (root mean squared error) exceeded 50 % [49]. Riad Akhundov et al. (2022), evaluated the effects of personalized models on kinematics, kinetics and musculotendon (MTU) dynamics over generic models from the same person. The joints centres, segments mass, inertia and isometric peak force of the subject-specific models were constructed based on subject lower limb MRI images, while generic models MTU proprieties were retired from literature and geometry was linearly scaled to each subject. The results demonstrated significative differences on joint kinematics and moments between models, subject-specific models presented lower muscle forces and activations, and more realistic fiber lengths and velocities, whereas in generic models, body segments, muscle masses and volumes were disparate from actual anatomy of the subject. Variability in maximum isometric muscle force between right and left limb was also observed in subject-specific models, promoting its use for studying patients with partially affected members [50].

Although, the advantages of models obtained with the aid of medical imaging are several, such as more realistic model proprieties, better simulation predictions and denoted intra and inter-subject variability, due to costs and time issues, the scaled-

generic models were the ones selected to be used in this work and as such the scaling of these models will be the focus of this review.

4.3. Geometrical scaling

The process of conversion of a generic model to a scaled-generic model, known as scaling, is associated to a reformulation of the model's initial base proprieties of geometry, inertia, and muscles to a specific subject, involving changes at level of the body segments, joints and musculotendon units. Alterations at geometry level (segment lengths, joint orientations, muscle attachment points) strongly influence the simulation results. Thus, it is important to pay attention to the accuracy of the parameters provided. There are several formulations that allow to scale these geometrical parameters, they are roughly distributed as: i) linear scaling; ii) non-linear scaling; iii) optimization-based scaling. The first approach, the linear scaling, adjusts the body segments dimensions and musculotendon lengths properties linearly by means of scale factors, computed by the ratio between the distances of a given pair of model markers and the corresponding pair of experimental markers on a given trial. On the other hander hand, non-linear scaling methods map the subject bone geometry and muscle path, reconstructing the reference model by means of non-linear transformations [51,52]. Lastly, in optimization-based scaling methods, used by simulations software like OpenSim, the parameters to be scaled are computed by reducing the least-squares error between model's markers positions and experimental markers positions that match the same anatomical landmark, over a selected time interval and motion [51].

Using two different non-linear scaling approaches to adapt the geometrical proprieties of a generic lower limb model, M. E. Lund et. al (2015) examined the output differences between these methods and linear scaling, and it´s sensitivity to the marker's positions. On both approaches a subject-specific stick-figure model is constructed from a standing reference pose, where the joint axes and segment reference frames are defined, and markers are placed. Resorting to non-linear functions, the generic model is scaled by assimilating the geometric specifications

defined on the stick-figure model. The difference between the two methods lies in the characterization of the joint parameters. While in one of the methods the hip joint center is computed trough regression equations (anatomical landmark scale model), in the other the joint locations are optimized using additional functional joint trials (Kinematically scaled model). The linear scaling model predictions are strongly influenced by markers placement on the subject, contrary to the other two methods. However, in all approaches, the muscle moment arms, muscle force and joint contact force are dependent on the model markers positions. The joint angles and moments profiles of the three models were similar with some differences on hip abduction/flexion moment, knee flexion moment, and ankle inversion/internal rotation angles and moments. Among them, the smallest variation in simulated knee joint contact force relative to measured forces from prosthesis was achieved on the Kinematically scaled model, although the results presented are not sufficient to conclude the superiority of a scaling method over the other [53].

In 2019, P. Puchaud et. al, studied the influence of the scaling method on kinematics, trough lower limb models with geometrical proprieties scaled with five different approaches: i) linear scaling (segment length factors); ii) image-based scaling; iii) linear scaling with optimization-based scaling (optimization of segments lengths, joints axes orientations, only selected markers coordinates) ; iv) linear scaling with optimization-based scaling (only optimization of joints axes orientations, all markers coordinates); v) image-based-scaling + optimization-based scaling (only joints axes orientations and all markers coordinates). The segment lengths, joint orientations, joint angles of linear and linear-optimization models were compared with the values of the reference image-based model, drawing the conclusion that model scaled with linear scaling plus optimized marker coordinates and joint axes orientations presented the best results. Although these results encourage the use of optimization-based scaling, as it contributes to minimize kinematic errors, its use in segment length scaling may have to be reconsidered, has its values were significantly different from the reference imaging data, while having particular attention to constraints and initial guess defined for the algorithm [51].

As mentioned before, since most scaling procedures rely on markers to access anatomical landmarks and joints axes, they are greatly influenced by placement of markers on subject body and the choices on model marker's locations [53].

4.4. Strength scaling

Apart from the geometrical scaling of a model, which involves the tuning of length, mass, inertia, orientations of segments, joints and musculotendon length proprieties to a subject's anthropometry, a muscle actuator in a musculoskeletal model is also defined by its peak force, usually derived from cadaveric studies. This propriety is usually overlooked when scaling the generic model, as its influence on simulation results is also controversial. However, having as objective the development of a highly user-specific model, special attention should be given to this parameter. A literature search was performed in Scopus and PubMed databases with the following keywords and Boolean operators: "strength scaling" AND "OpenSim" OR "Musculoskeletal model"; "force scaling" AND "Musculoskeletal model". Out of the few results, only the more relevant for this work were chosen, i.e., articles with focus on upper-limb models, scaled-generic models, and influence of force scaling on simulation outputs. Therefore, out of the documents found, only 5 studies that met the selection criteria were chosen.

4.4.1 Results

Over the years, several studies have tried to scale this force using different methods and studied its influence on simulation output. Overall, these methods are based on subject physical characteristics like height and weight, muscle volume, or optimization algorithms based on experimental measurements of force or torque (Table 3).

Table 3- Strength scaling methods review

Study	Model	Method	Equipment	Validation	Outcomes

J.M. de Vet et al. (2021) [54]	Thoracoscapular Delft shoulder and elbow model (TDSEM);138 muscle-elements	Muscle volume-isometric force	Force-transducer	Maximum directional forces and moments measured during MVIC (Maximum voluntary isometric contraction) trials	The applicability of this method in population with lower force or higher force generating capacities is not tested
Charles et al. (2020) [49]	Lower limb musculoskeletal models (pelvis, legs, feet); 92 musculotendon unit actuators	Muscle volume-fiber length; Body mass	Siemens 3.0 T Prisma scanner; Isokinetic dynamometer	Joint torques measured in isokinetic and isometric conditions	The scaling by mass and length did not reveal significative differences compared to generic models. Not tested for upper-limb models
F. D. Maso et al. (2016) [55]	Upper-limb EMG-driven musculoskeletal model (scapula, arm, forearm); One DOF-flexion/extension of forearm. 4 muscles units.	Optimization-based algorithm (joint torque)	EMG sensors; 3D force and torque sensor (SH2653-1106B3, Sensix, Poitiers, France)	Force, torque, and muscle excitation (biceps brachii short head, brachioradialis, brachialis, triceps brachii long head) from three elbow MVIC.	Using a specific assortment of MVIC trials, the smallest RMSE between predicted and computed joint torques was 7.4 %.
Correa and Pandy (2011) [56]	Opensim generic gait model; 10 body segments, 23 DOF, 92 muscle-tendon units	Body mass-musculotendon length	Motion capture system (VICON, Oxford Metrics Group, Oxford, UK, 100 Hz); 6 strain-gauged force plates (AMTI, Watertown, MA, USA, 1000 Hz)	peak isometric muscle forces computed from MRI	The muscle forces patterns estimated by the scaled model were close to those predicted by the MR-based model during walking. Further research is needed to verify the correlation between muscle volume and body mass on upper-limbs models.

Goislard de Monsabert B. et al. 2017 [57]	hand model (five fingers and wrist); 23 DOF and 42 muscles	Optimization-based algorithm (net joint moments)	torque sensor (DR2112 50 Nm, SCAIME, Juvigny, France). Surface EMG data (MP150, Biopac Systems Inc., Goleta, CA) (Disposable Ag/AgCl surface electrodes 8 mm diameter).	Correlation between measured net joint moments and estimated muscle moment capacities; Muscle activations and external forces determined from power grip tasks	The method proposed was able to represent differences on force capacities between subjects.

4.5. Mass-length, muscle volume-based methods

Within the selected studies ,presented in the Table 3, three are based on the relationship between mass, muscle volume and muscle fiber-tendon length. The first method, translated by equation (1), was developed by Correa and Pandy (2011) and is based on mass-length relationship, by assuming that muscle volume is proportional to total body mass and muscle-fiber length to musculotendon length, scaling muscle´s maximum isometric force by the product of these variables and the generic peak isometric force defined on the model [56].

$$F_{max}^{scaled} = F_{max}^{generic} \times \frac{M^{scaled}}{M^{generic}} \times \frac{l_{MTU}^{generic}}{l_{MTU}^{scaled}} \qquad (1)$$

The forces estimated by lower limb models scaled with this method and by models based on MRI images have shown same behaviour during walking and non-expressive statically differences between values, where on both models the inertial properties, optimal muscle-fiber lengths and tendon slack lengths, joint locations and

orientations were adjusted to each subject by scaling factors based on body mass and MRI images, respectively. These outcomes present this method as a possibility for use when studying models of children but does not give guarantees for populations with other age groups, health status, motions, or models of other body parts [56]. Hernandez V. et al. 2015,2018 utilized this method to scale the peak muscle force on upper-limb musculoskeletal model, and N. Rezzoug et al. 2019, additionally, attributed a factor of 0.5 to this formulation for female subjects, having obtained favourable results on young healthy population [58, 59, 60].

Years later, James P. Charles et al. (2020), investigated the accuracy in estimating muscle torque with respect to experimental data of five lower limbs models containing different muscle properties. All models were constructed from MRI and Diffusion tensor imaging (DTI), featuring the same bone geometry and muscle paths, but with variations on muscle-force generating proprieties (optimal fiber length, tendon slack length, pennation angle and maximum isometric force). One of the models contained properties derived from MRI, while in the others these arose from generic data of elderly or young population, with two models for each population type. Regarding these four models, two of them, one for each population, use a mass law between the body mass of each subject ($M^{subject}$) and the body mass of a generic model ($M^{generic}$) to scale maximum isometric force (equation 2), in addition to an optimization algorithm to determine the values of fiber and tendon length based on subject anthropometry [49].

$$F_{max}^{scaled} = F_{max}^{generic} \times \left(\frac{M^{subject}}{M^{generic}}\right)^{(2/3)} \qquad (2)$$

Overall, the knee muscles torque estimated by the models derived from MRI had the most accuracy. However, the models scaled with generic young data exhibit similar comportment and the rmse differences between them were smaller. Although, the optimization of muscle architecture derived from cadaveric studies of elder population contributed to improve the results, the scaling by mass, and optimization of

muscle force-length proprieties of young data did not reveal significative differences when compared with models with generic data without optimization, given that the subjects on this study had similar age and mass as the generic data selected. The results also suggested that these young generic models may only be reliable for people with lower strength, as the rmse value varied as per subject, reinforcing the need to develop individualised models capable of showing inter-subject variability [49].

Lastly, in 2021, J.M. de Vet tried to scale strength proprieties based on the correlation between subject's mean maximum force in isometric and/or isokinetic strength trials and total muscle volume, obtaining a subject-specific upper-limb model. The total upper muscle volume is estimated based on its linear relationship with mean maximum force, reported on a study by Bart Bolsterlee et al. (2015, [61]). This volume is used to calculate a scale factor in relation to total upper-extremity muscle volume of the generic model. The scaled muscle-element volume ($v^{m,sc}$) is then obtained by multiplying this scale factor by the generic muscle-element volume. Finally, the specific peak isometric muscle force ($F_{max}^{m,sc}$) is determined by the product between scaled muscle volume ($v^{m,sc}$), scaled muscle's optimal fiber length ($l_0^{m,sc}$), optimal pennation angle (α_0^m) and muscle specific tension (σ_{max}^{sc}) , expressed on equation (3) [54].

$$F_{max}^{m,sc} = \frac{v^{m,sc} \times \cos(\alpha_0^m)}{l_0^{m,sc}} \times \sigma_{max}^{sc} \quad (3)$$

Although it is not possible to experimentally validate the individualized muscle force, it may be a possible method to scale upper-extremity models, with exception for population with non-uniform muscle force distribution like elderly or athletes [54].

4.6. Torque based methods

In addition to scaling methodologies based on the proportionality between mass and length, there are also studies that resorted to the use of optimization

algorithms, by computing factors or variables that meet the best value of the objective function, in this case the minimization of the moments.

In 2016, Fabien Dal Maso et al. estimated maximum muscle isometric force (equation 4) by multiplying physiological cross-sectional area (PCSA) of each muscle extracted from literature and a product of two variables (w_m, σ_{max}) ,computed trough minimizing the rmse between predicted joint torques (Q_{EMG}) obtained via an electromyographic-driven musculoskeletal model and computed torques (Q_{INV}) from inverse dynamics (equation 5) , using several combinations of elbow flexion and extension MVIC trials [55].

$$F_{max}^{iso} = w_m \times \sigma_{max} \times PCSA_m \quad (4)$$

$$\min_{w_m, \sigma_{max}} \frac{1}{2} \int \left(Q_{EMG}(t) - Q_{INV}(t)\right)^2 \quad (5)$$

The best combination presented a rmse between predicted and computed torques of 7.4 %. This method decreased the error relative to previous ones. However, this study uses an upper-limb model with only one DOF of the elbow joint, not representing the physiological joint with 2 DOFs and true physiological values of muscle's maximum muscle stress (σ_{max}) [55].

Goislard de Monsabert B. et al. (2017), also proposed an optimization algorithm (equation 6) centered on minimizing the difference between net joint moments estimated by a model ($\widehat{M}_{ergo}^{j}$) and experimentally measured (M_{ergo}^{j}) on MVIC trials of wrist and hand joints. The estimated joint moments are function of muscle specific tension (σ_{max}), scaling factor per muscle group (c^g), and the estimated mechanical activation in a certain task per muscle group ($a_{mech}^{g}(n)$). The maximum isometric force (equation 7) is then individualized by multiplying the muscle PCSA value from literature and σ_{max} , c^g resulting from the optimization procedure [57].

$$f\left[\sigma_{max}, c^g, a^g_{mech}(n)\right] = \sum_n \left\{M^j_{ergo}(n) - \widehat{M}^j_{ergo}\left[\sigma_{max}, c^g, a^g_{mech}(n)\right]\right\}^2 \quad (6)$$

$$F^m_{max} = c^g \times \sigma_{max} \times PCSA^m \quad (7)$$

The quantities estimated, like muscle forces, with this force scaling method demonstrated strength variability between subjects, whether they are old, young or athlete, contrary to the initial model. Further investigation regarding the muscle force-length relationship and its use in other types of musculoskeletal models is required since it was not included in this procedure [57].

Despite the uncertainty of the impact of scale strength on simulation results, since the conclusions differ between studies and muscle strength is difficult to validate directly, it is one of the model muscle definition parameters that can be changed and contribute, even if slightly, to approximate more the generic model to a specific user. The body mass-length force scaling methods have a straightforward implementation and formulation. Notwithstanding, through them, it might be difficult to exhibit strength differences between subjects and muscles with opposite functions, additionally its efficacy depends on the geometrical parameters scaled previously. On the other side, the torque-based optimization algorithms may be more concise in reflecting inter and intra-subject muscle strength variability but are generally more delaying and highly dependent on algorithm formulation, constraints, and initial conditions.

5. Methodology

This chapter describes the scaling approach used in this study in order to adjust the generic model to a user-specific model and analyze the influence of scaling methods. Starting by scaling the geometrical proprieties according to subject´s anthropometric data, customization of the model strength is then performed by tuning

peak isometric muscle force value, culminating on a final model with both geometrical and force proprieties fit to each user.

5.1. Scaling methodology

The scaling of the model is an essential step to do before starting any simulation, as this process alters joint positions, muscles fibers and tendon proprieties that influence further calculations of muscle forces, activity, joint moments, and torque [32,34]. On this work, the conversion of a generic model to a user-specific model will be sub-divided in two major processes: geometrical scaling and force scaling (Figure 16).

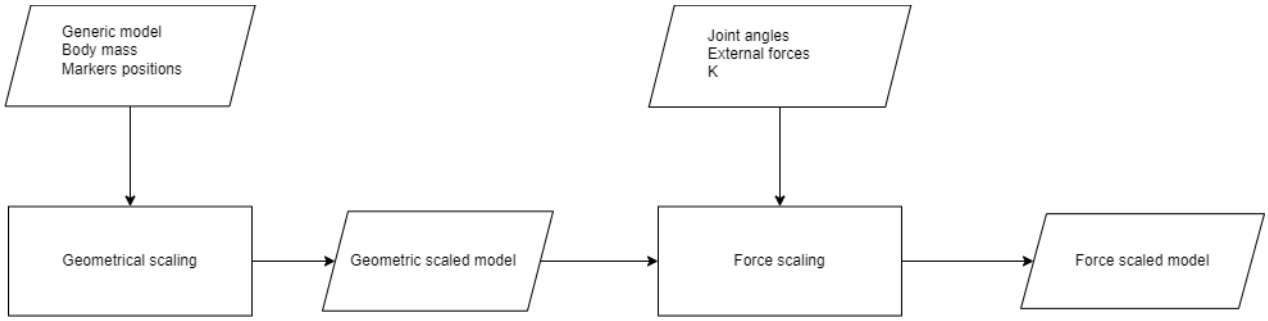

Figure 16 - Model scaling methodology.

This methodology consists briefly in transforming the generic model in a geometrical scaled model trough geometrical scaling process by adjusting anthropometry, mass and musculotendon length proprieties using OpenSim Scale tool. Then this new model will serve as input to the force scaling process, in addition to the joint angles, external forces applied on the movement performed by the subject, and an additional variable *k* that is dependent on the force scaling method applied, described later in this chapter. Finalizing this process, the resultant output is a model specific to the user, in both anthropometry and strength.

5.1.1. Geometrical scaling

The geometric scaling is essential to compute precise orientation and position of joints and body segments, as well as its kinematics and proportions. In Opensim the model body segments are scaled uniformly or disparately for each direction of the coordinate system by applying scale factors, that may be obtained by measurement-based or manual scaling. The scaling factors attained by the first scaling method correspond to the ratio between the distance of the model's markers pairs and the distance of the pairs of experimental markers that refer to the same anatomical positions. Concluded the process of scaling the dimensions of the segments, the model virtual markers are moved to match the positions of the experimental markers in a static pose. This pose is computed by minimizing the least-squares error between virtual markers locations and experimental markers positions provided in a file, over a selected time interval. The weight of each marker and coordinate are used to determine how strongly the algorithm should try to match them. The greater the weight the stronger the algorithm should match the experimental value more closely [62,63]. The overall scaling process is represented in Figure 17.

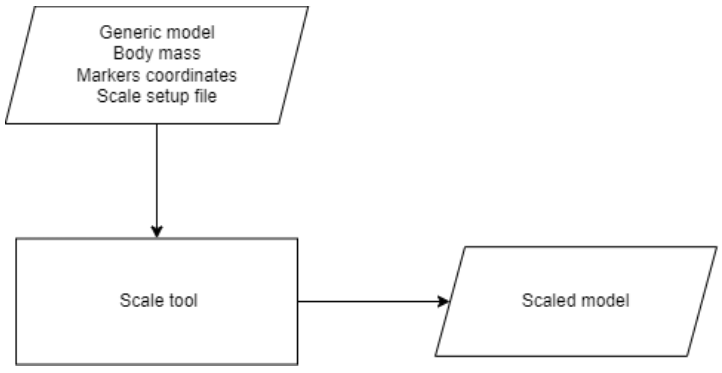

Figure 17 - Geometrical scaling process.

To perform the scaling process in OpenSim is required at least four inputs: a generic model containing markers; the experimental coordinates of markers from a static trial; the scaled model's mass; a setup file with the definitions of the scale factors and weights to be assigned to the markers to perform markers-based optimization scaling. Additionally, can be include a file with experimental joint angles of the same trial.

First, the markers x-y-z coordinates and motion joint angles were obtained by Xsens motion capture system, and further converted to Opensim file format (trc and mot) using Mokka (Mokka 0.6.2, Motion Kinematic & Kinetic Analyzer, Arnaud Barré 2009-2013) and Matlab software (Matlab R2021b, The MathWorks, Inc.). Due to difference in the global coordinate frame on OpenSim and Xsens, it was necessary to apply a rotation matrix of -90 degrees around x-axis on marker position data. The model markers (28 markers) were placed and named in agreement with anatomical landmarks of Xsens markers for upper limbs, torso and head, since the model is only of the upper body (Figure 18).

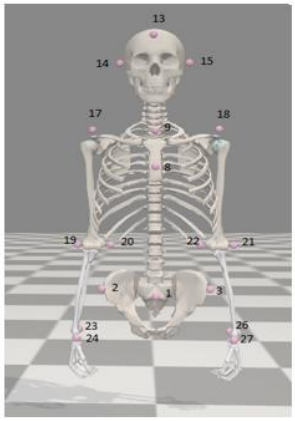

Model markers	
1 pHipOrigin	15 pLeftAuricularis
2 pRightASI	16 pBackOfHead
3 pLeftASI	17 pRightAcromion
4 pSacrum	18 pLeftAcromion
5 pL5SpinalProcess	19 pRightArmLatEpicondyle
6 pL3SpinalProcess	20 pRightArmMedEpicondyle
7 pT12SpinalProcess	21 pLeftArmLatEpicondyle
8 pPX	22 pLeftArmMedEpicondyle
9 pIJ	23 pRightUlnarStyloid
10 pT4SpinalProcess	24 pRightRadialStyloid
11 pT8SpinalProcess	25 pRightOlecranon
12 pC7SpinalProcess	26 pLeftUlnarStyloid
13 pTopOfHead	27 pLeftRadialStyloid
14 pRightAuricularis	28 pLeftOlecranon

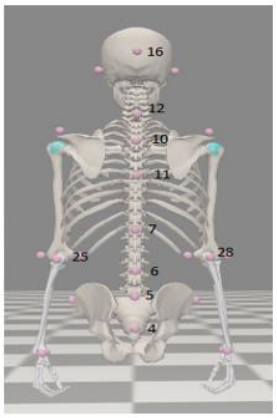

Figure 18 - Model´s markers.

Opensim documentation recommends not use all markers from motion-capture system to position and scale the model, only markers that match anatomical landmarks and functional joint centres [32,65]. Within the experimental markers, the ones that represented anatomical landmarks on arms, sternum, pelvis, and head were

chosen to track and model markers were to match these positions. Each marker was given a tracking weight of one since markers' location reliability is the same for all (Table 4). The markers placed on hands and spinal column were excluded since they do not include movable joints on this model.

Table 4 - Tracking markers and respective weight

Marker Name	*Weight*
pIJ	1
pPX	1
pRightAcromion	1
pLeftAcromion	1
pTopOfHead	1
pRightAuricularis	1
pLeftAuricularis	1
pRightASI	1
pLeftASI	1
pSacrum	1
pRightArmLatEpicondyle	1
pRightArmMedEpicondyle	1
pRightUlnarStyloid	1
pRightRadialStyloid	1
pRightOlecranon	1
pLeftArmLatEpicondyle	1
pLeftArmMedEpicondyle	1
pLeftUlnarStyloid	1
pLeftRadialStyloid	1
pLeftOlecranon	1

5.1.2. Force scaling

The OpenSim scale tool allows the adaptation of model´s geometry, mass and musculotendon length proprieties between subjects, however doesn´t consider the inter-subject variability of muscle strength. As described in chapter 4 there are various methods to scale the peak isometric force, ranging from a simple equation or more complex mathematical optimization. To test the influence of the scaling method on the determination of the muscle force/muscle activation, three methods presented in the literature were selected and additionally an optimization algorithm was developed. The formulations selected from literature are summarized on the Table 5.

Table 5 - Scaling methods from literature

Author	Formula
James P. Charles et al. (2020) [49]	$F_{max}^{scaled} = F_{max}^{generic} \times \left(\frac{M^{scaled}}{M^{generic}}\right)^{(2/3)}$
Correa and Pandy (2011) [56]	$F_{max}^{scaled} = F_{max}^{generic} \times \frac{M^{scaled}}{M^{generic}} \times \frac{l_{MTU}^{generic}}{l_{MTU}^{scaled}}$
Steele et al. (2012b) [66]	$F_{max}^{scaled} = F_{max}^{generic} \times \left(\frac{H^{scaled}}{H^{generic}}\right)^{2}$

Where (M^{scaled}) corresponds to the total body mass of each subject, and ($M^{generic}$) to the body mass of the generic model, l_{MTU}^{scaled} to the scaled musculotendon length, l_{MTU}^{genric} to musculotendon length before scaling the generic model, H^{scaled} to the height of the subject and $H^{generic}$ to height of the model by definition. Analyzing the three formulas it is possible to observe that the scaled maximum isometric force(F_{max}^{scaled}) is given by means of multiplying a factor to the maximum isometric force originally set on the model ($F_{max}^{generic}$), whether it is determined by ratios of mass, height or mass-length.

In addition to those methods a muscle activation-based optimization algorithm was developed, that can be resumed on the following flowchart.

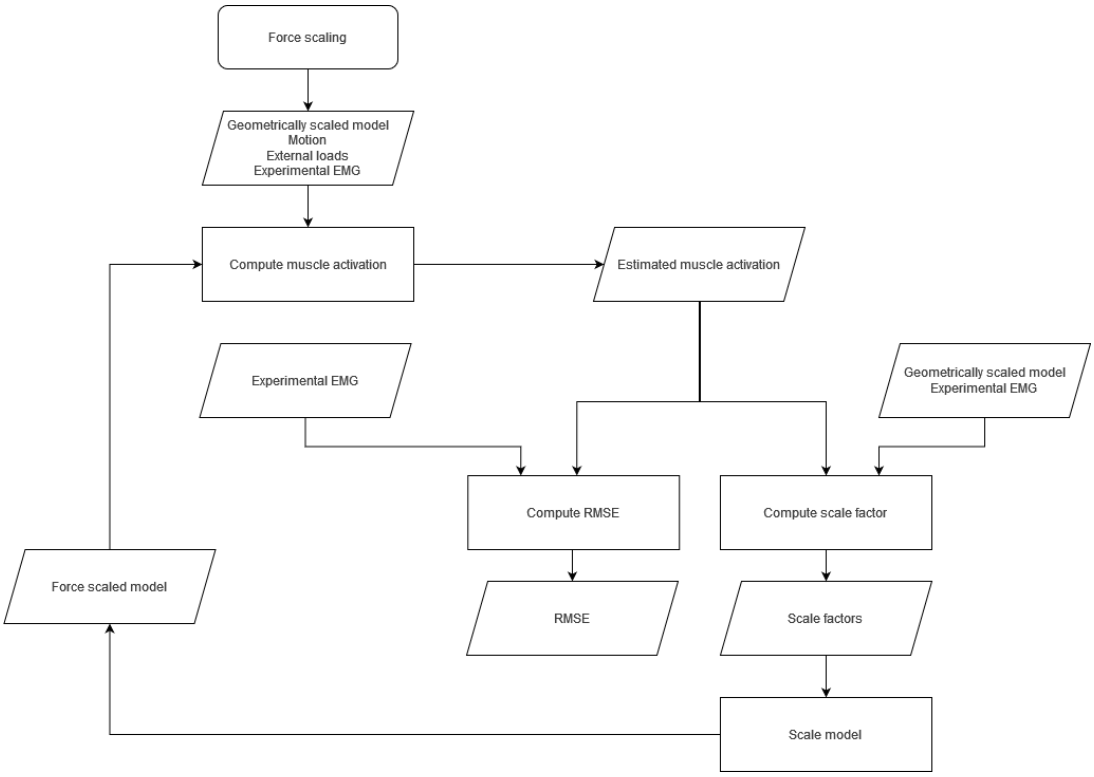

Figure 19 - Flowchart of muscle activation-based optimization algorithm to scale model strength.

This algorithm was implemented in Python ver. 3.8.13, having been created four main functions:

- **Compute muscle activation**- estimates the muscle activation by providing the respective inputs: model, kinematics, loads, experimental EMG, initial and final time to solve the problem.
- **Compute scale factor**- obtains the scale factor or scale factors trough solving of an activation-based optimization problem.
- **Scale model** – scale the strength proprieties of the given musculoskeletal model, multiplying the model´s peak isometric force by the obtained scale factor (s).
- **Compute RMSE**- calculates the mean RMSE between predicted and experimental activations of the supplied muscles.

The algorithm starts by computing the initial muscle activations that may have originated the input kinematics and kinetics. This type of muscle redundancy problem is solved using OpenSim Moco tool's "MocoInverse", which by providing the joint angles, forces, musculoskeletal model it is possible to find the resultant activation per frame rate for each model's muscle, known as inverse dynamics methods. Within this tool is added other class, known as "MocoControlTrackingGoal" that will track the prescribed experimentally measured normalized EMG, by minimizing the sum of squared differences between experimental and predicted activations [67,68]. Once this step is completed, follows the determination of the scaling factor(s) that will change the maximum isometric force of the muscle, through an activation-based optimization algorithm, implemented using Python optimization library "pymoo" [69]. An optimization problem is defined by the variables to be determined known as decision variables, in this case the scale factor(s), the objective function to be maximized or minimized, and by limits and constraints that condition it. Assuming that the normalized experimental activation (a_{exp}) (range from 0 to 1) per muscle can be expressed as the product between Moco's estimated muscle activation (a_{est}) and a factor (S), according to equation 1, then the difference between the two variables has to be equal to zero. This is the premise that defines the objective function of the optimizer, that is to minimize the squared difference between the sum of experimental and predicted activation of selected muscles (from 1 to n) over an instant (t) within the time interval selected (ti to tf), translated by equation 2. The scale factor of force (S) to compute, was defined as being bounded inferiorly and superiorly by values of 0.1 and 10, respectively, which represents a variation of strength capacity between values that are 10 % weaker and 1000 % stronger than the original model.

$$a_{exp} = S \times a_{est} \iff a_{exp} - S \times a_{est} = 0 \qquad (1)$$

$$minimize: \left(\sum_{mu=1}^{n} a_{exp}^{mu}(t) - \sum_{mu=1}^{n} S_i \times a_{est}^{mu}(t) \right)^2, mu = 1 \dots n, t \in [ti, tf] \quad (2)$$

$$subject\ to: 0.1 \leq S_i \leq 10,\ i = 1 \dots N$$

$$F_{iso,max}^{scl} = S \times F_{iso,max}^{gen} \qquad (3)$$

The optimal solution corresponds to the value of scale factor (S) that generates the minimum difference between activations, this value (equation 3) will be then multiplied by isometric maximum force of previously geometrically scaled model ($F_{iso,max}^{gen}$) obtaining then the scaled isometric peak force ($F_{iso,max}^{scl}$). This new force scaled model is then used as input to Moco, including the same motion, experimental activations and external loads defined initially, and muscle activations are again computed. Finally, the RMSE between this new estimated activation and experimental EMG is calculated and registered, and cycle is replicated until the initially defined number of iterations is reached. Each RMSE and scale factor(s) computed per cycle is registered and saved in a text file.

In order to test the influence of scaling factor dimensions, i.e., scaling the model with a single unique factor for all the muscles or determine multiple scale factors assigned to each muscle, variations were made in the problem formulation, while keeping S as the variable to compute, the same variable bounds and premise of the objective function. Given this, three formulations were made:

- First: one variable, single-objective optimization
- Second: multivariable, single-objective optimization
- Third: one variable, multi-objective optimization.

In the first formulation, a single scale factor (S) is determined and used to scale all the muscles on the model, by minimizing the objective function translated by equation 4.

$$minimize: f(S) = \left(\sum_{mu=1}^{n} a_{exp}^{mu}(t) - \sum_{mu=1}^{n} S \times a_{est}^{mu}(t) \right)^2$$

$$subject\ to: 0.1 \leq S \leq 10 \qquad (4)$$

The second problem involves the minimization of a single goal from the optimization of more than one decision variable, whose dimension (*i*) is corresponding to the number of muscles (*mu*) experimentally analysed (equation 5). This contributes to uneven scaling of the model, where each of the given group of factors will only be applied to the muscle that has been associated with it.

$$minimize: f(S) = \left(\sum_{mu=1}^{n} a_{exp}^{mu}(t) - \sum_{mu=1}^{n} S_i \times a_{est}^{mu}(t) \right)^2, mu = 1 \dots n, i = 1 \dots n$$

$$subject\ to: 0.1 \leq S_i \leq 10 \qquad (5)$$

The third formulation (equation 6) is similar to the first one with the respect of number of unknown variables, however it differs on the number of objectives to minimize. Unlike, the other formulations presented above that are based on the experimental and estimated muscle activations of a single movement executed by the subject, this problem is projected considering the different stimulations of the muscles according to the mobility of the joint in multiple directions. Therefore, the number of goals (*i*) is defined by the number of motions selected to analyse, which result on a single solution that represent the minimum possible difference between activations for that association of movements.

$$minimize: f_i(S) = \left(\sum_{mu=1}^{n} a_{exp}^{mu}(t) - \sum_{mu=1}^{n} S \times a_{est}^{mu}(t) \right)^2, i = 1 \dots j$$

$$subject\ to: 0.1 \leq S \leq 10 \qquad (6)$$

The addition of these three optimization-based proposals with the mass-length approaches addressed in the beginning of this subchapter, gives a set of six force scaling methods to analyse on this work, summarized on the table below. To simplifying the process of data discussion, for each method were attributed letters of identification.

Table 6 - Force scaling methods

Scaling method	Name	Formula
Mass	M	$F_{max}^{scaled} = F_{max}^{generic} \times \left(\frac{M^{scaled}}{M^{generic}}\right)^{(2/3)}$
Mass-length	ML	$F_{max}^{scaled} = F_{max}^{generic} \times \frac{M^{scaled}}{M^{generic}} \times \frac{l_{MTU}^{genric}}{l_{MTU}^{scaled}}$
Height	H	$F_{max}^{scaled} = F_{max}^{generic} \times \left(\frac{H^{scaled}}{H^{generic}}\right)^{2}$
Muscle activation-based optimization (single variable-single objective)	SS	$F_{max}^{scaled} = F_{max}^{generic} \times S$ $min\, f(S)$
Muscle activation-based optimization (multi variable-single objective)	MS	$F_{max}^{scaled} = F_{max}^{generic} \times S_i\,, i = 1 \dots n$ $min\, f(S)$
Muscle activation-based optimization (single variable-multi objective)	SM	$F_{max}^{scaled} = F_{max}^{generic} \times S$ $\min f_i\,(S), i = 1 \dots n$

5.2. Experimental validation

With the purpose of studying the influence of these scaling methods on simulation results, an experimental protocol was formulated. The protocol was divided into two parts, the first half was defined with the goal of calibrating the musculoskeletal model, while the second half concerns the validation of the force scaling approaches.

5.2.1. Participants

The study sample was non-probabilistic, according to the selection criteria: age between 18-40 years; without health issues at neurological, cardiovascular, or musculoskeletal level. Five healthy participants were recruited to the experiment (gender: 3 females and 2 males, age: 23.20 ± 3.49 years, height: 1.66 ± 0.11 m, body mass: 60.80 ± 12.74 kg), and respective personal and anthropometric data (age; height; body mass; gender; upper arm length; forearm length; shoulder width) were registered (Table 7). All subjects gave their informed consent for inclusion before their participation.

Table 7 - Age (years), Gender (female/male), age (years), body height (m) and body mass (kg) for each participant

Subject	Age (Years)	Gender (F/M)	Body Height (m)	Body Mass (kg)
1	23	F	1.612	49
2	26	F	1.7	63
3	32	M	1.74	68
4	24	M	1.76	77
5	26	F	1.5	47

5.2.2. Data acquisition

The joints kinematics were recorded using 17 Xsens IMUs sensors (Xsens MTw Awinda, Xsens Technologies, Enschede, The Netherlands) on upper and lower body, with a sampling rate of 60 Hz. They were placed on the designated suit and fixed in place with hook and loop straps and duct tape on the head, sternum, right shoulder blade, left shoulder blade, left upper arm, right upper arm, left forearm, right forearm, right hand, left hand, pelvis, left upper leg, right upper leg, left lower leg, right lower leg, left foot, right foot. Muscle electrical activity was captured by wireless surface EMG sensors (Delsys Trigno^{TM} Avanti Platform, Massachusetts, USA), with a sampling frequency of 2100 Hz. A total of eight sensors were placed according to SENIAM [70] positioning recommendations, for each one of the eight muscles: *Biceps brachii* (two heads), *Triceps long head*, *Triceps lateral head*, *Brachioradialis*, *Pectoralis major*, *Deltoid anterior*, *Deltoid middle* and *Deltoid posterior*. The force exerted by the participants during the first part of the protocol, was translated by a strain gauge load cell capable of reading a weight value up to 20 kg in one-direction while in compression and tension, and subsequent characteristics: Repeatability Error Max: ± 10 g; Cell Non-Linearity Max: 10 g; Cell Hysteresis Max :10 g. Accoupled with a load cell amplifier (HX711) 24-bit analog-to-digital converter (ADC) with 10 samples per second output data rate and gain of 12. This amplifier was connected to an 8-bits microcontroller (ATMEGA8) by a two-wire interface (clock and data), as shown in Figure 20. The trials were executed after synchronization of EMG, Xsens and force acquisition systems.

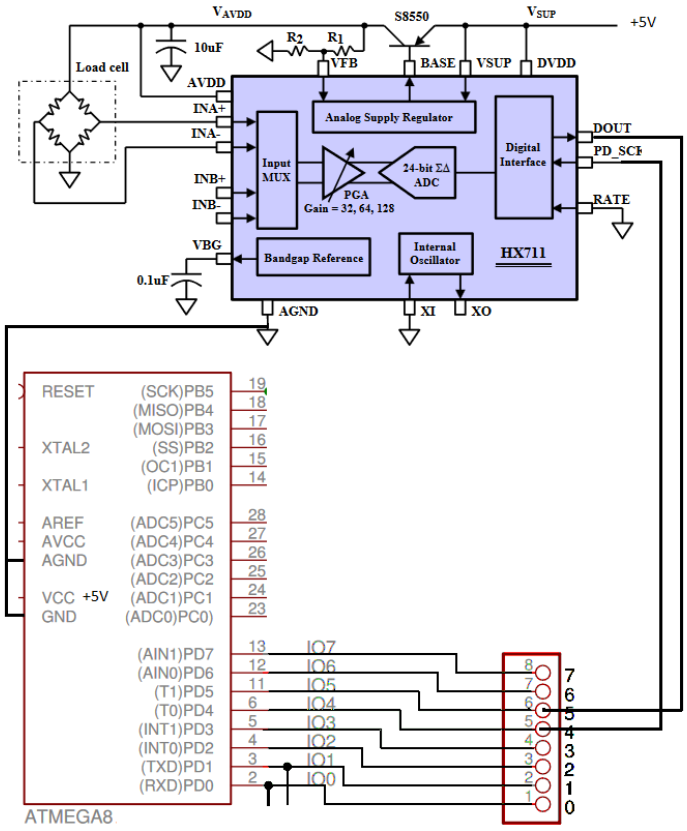

Figure 20 - Load cell amplifier (HX711) with microcontroller (ATMEGA8) circuit diagram [71,72].

5.2.3. Experimental Procedure

Firstly, after skin preparation and placement of EMG sensors (Figure 21), MVC (maximum voluntary contractions) were performed with the dominant arm for each one of the eight muscles selected to be analyzed. 3 repetitions with a 60 s interval in between were executed for each muscle. Terminated the MVIC acquisition, IMUs sensors were placed on the respective suit (Xsens MTw Awinda, Xsens Technologies, Enschede, The Netherlands) worn by the subject (Figure 21). The Xsens full-body model was then configured for each participant by the providing anthropometric measures, and further calibrated on MVN Studio software (MVN studio software, Xsens Technologies).

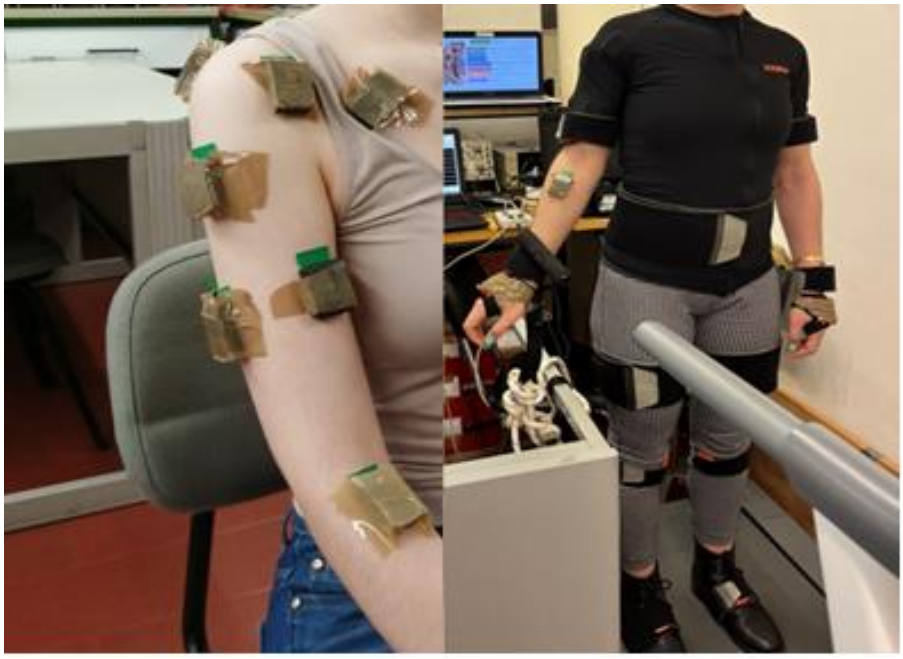

Figure 21 - Placement of EMG sensors (left) and Xsens suit with IMUs sensors (right).

Then, the protocol was executed sequentially, according to following order: 1) Elbow flexion, shoulder flexion and shoulder abduction movements; 2) point to point tasks. The first part of the protocol aims to scale the strength of the model for each subject, consisting in the measurement of muscle myoelectric activity and total muscle force exerted during the execution of three different isolated upper limb movements: elbow flexion, shoulder flexion and shoulder abduction.

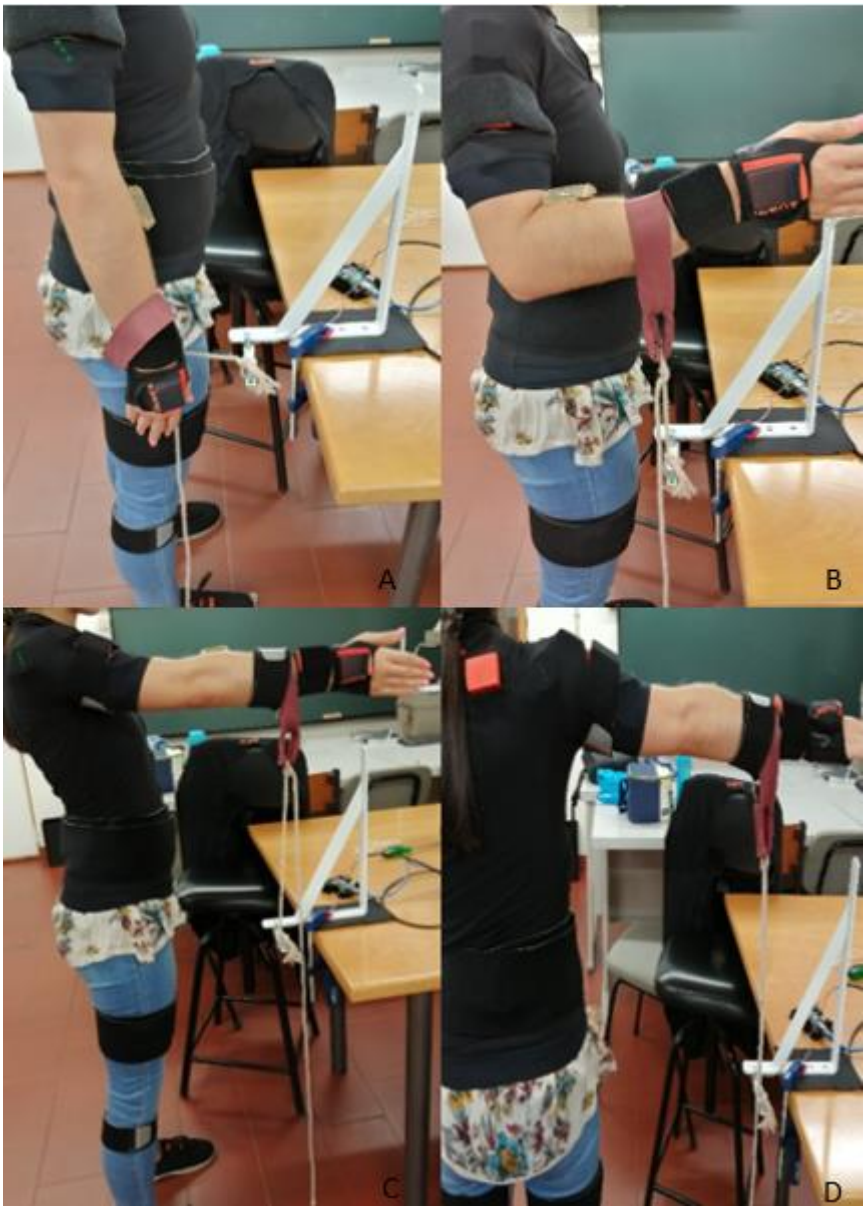

Figure 22 - Part I of protocol. Start pose (A), Elbow flexion (B), Shoulder flexion (C), Shoulder abduction (D).

As exemplified on Figure 22 , the survey participants start on n-pose (shoulder flexion: 0°, shoulder abduction: 0°, elbow flexion: 0°) and maintain this posture 5 seconds, then after this period the maximum force is exerted with dominant arm, holding 3 seconds, while performing the isometric movement of the upper limb (shoulder flexion: 90° or shoulder abduction: 90°, elbow flexion: 90°) with upright posture, finishing with the return to the neutral position. Each movement is repeated five

times, with an interval of 60 seconds amid each recurrence, and 2 minutes between movements, giving a total of 15 trials per subject.

The second half of the protocol aims to validate the force scaling methods presented earlier, through recording of EMG signals during a continuous motion with a diversified shoulder joint mobility. This part of the protocol was based on a study by Robert M. Mira et al. (2021) [73]. The setup consists of circumference with a radius of 30 cm with nine red points (Figure 23), that represent the circumference center (O), the four cardinal directions (N, S, W, E) and four intercardinal directions (NE, NW, SE, SW) of compass rose. This circumference was secured on the wall so as to face the subject while executing the exercise in a standing position.

Figure 23 - Part II of protocol. Circumference of radius 30 cm and center O.

The first 5 seconds are identical to the first part of the protocol, staring with same pose, afterwards the subjects lift the dominant arm, where the EMG sensors are placed, moving pointer to the center of target set (O) and keep it two seconds,

proceeding then to appoint to target (NE) and maintain that position for two seconds, then return to center (O) and hold two seconds with straight posture. Repeating the same procedure to the next targets (E, SE, S, SW, W, NW, N) in clockwise direction, with the last being (O). This exercise is reproduced three times, with a break of 60 s between each repetition.

5.2.4. Data processing

The force data was registered by software CleverTerm [74] through communication of serial port from microcontroller to computer, and posteriorly saved on a text file with time and weight data columns. This file was then formatted according to Opensim file structure (force, application point, torque) and resampled to 60 Hz with self-made python code. The joint angles and virtual markers were exported in MVN Analyze (Xsens Technologies, Enschede, The Netherlands) to mvnx and c3d file format, respectively. Then, the mvnx files were used as input of a MATLAB (version R2021a) script, which converts Xsens joint angles to Opensim coordinate system and exports the resultant angles on a mot file, with header, column labels and data formatted according to Opensim and model's joint definitions. The markers 3D coordinates were exported to trc file trough import of the c3d files on Mokka software, and further transformed to the model coordinate system in the OpenSim interface. The raw EMG signals were exported using EMGworks® Analysis (EMGworks®, Delsys) and normalized with the MVC signals via a custom python program.

5.2.5. Statistical analysis

The statistical analyses were performed using JASP software version 0.16.4 (JASP, University of Amsterdam, Netherlands). To study the differences between force scaling approaches, paired samples t-tests were performed for parametric data. The respective assumptions were evaluated: (1) data Independence (2) data normality, trough Shapiro-Wilk test; (3) existence of outliers. The equivalent non-parametric

Wilcoxon signed-rank test was executed when assumptions were violated. The statistical tests were conducted with a confidence level of 95% (α=0.05).

6. Results and Discussion

6.1. Preliminary trials and results

Experimental data, namely joint angles, external forces, and EMG were collected from one individual (gender: female, age: 26 years, height: 1.50 m, body mass: 47 kg) while executing isometric elbow flexion, and further used as input data for simulation software tests. The experimental protocol was similar to the first part of the protocol presented in chapter 5, but only executed for the elbow flexion movement. Starting by adjusting the geometrical proprieties of the generic upper body model to the subject, a muscle redundancy problem was solved using *MocoInverse* tool by providing the corresponding kinematics and external loads files. The time interval defined for running the simulation corresponds to the duration of the isometric contraction, in which the elbow joint angle is constant, and the maximum force is exerted. The tool prediction accuracy was then explored by comparing the obtained muscle activation against measured EMG.

The experimental (orange) and estimated activations (blue) curves of nine muscles: *Deltoideus Anterior*, *Deltoideus Medius*, *Deltoideus Posterior*, *Pectoralis Major*, *Biceps Brachii* (long head), *Biceps Brachii* (short head), *Brachioradialis*, *Triceps Brachii* (long head), *Triceps Brachii* (lateral head), are shown on Figure 24. To establish a comparison between values, the experimental activations were normalized to peak value of MVC for each of the nine muscles selected, where both heads of *Biceps Brachii* were assumed to exhibit the same experimental activation. The computation

time for the estimated activations during a trial of 3.5 seconds was 47 minutes using an intel® core ™ i5-4210U CPU @ 1.70 GHz 2.40 GHz.

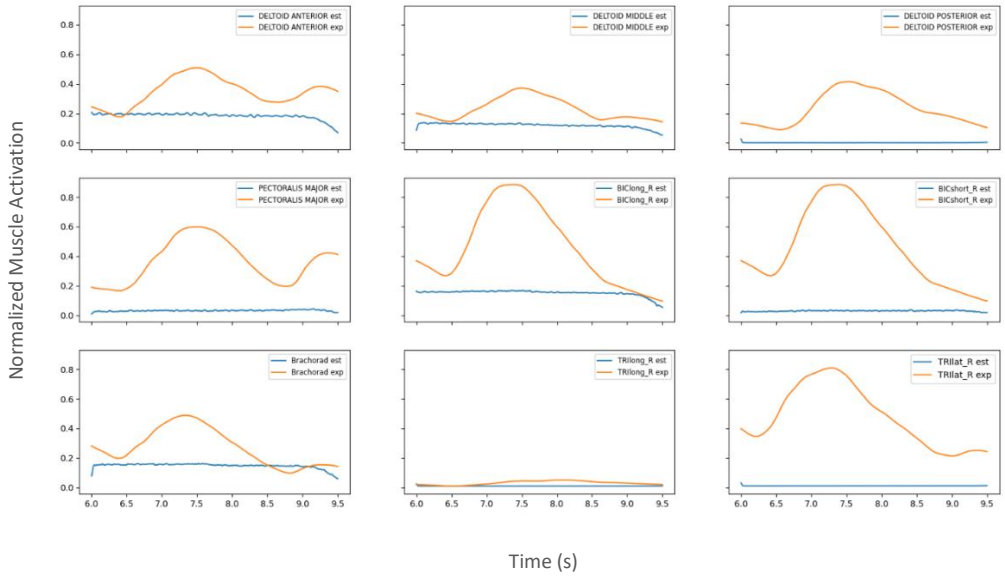

Figure 24 - Normalized experimental (orange) and estimated (blue) muscle activations during execution of maximum isometric force (6.0 s to 9.5 s), obtained by *MocoInverse* tool.

Observing both curves for each muscle, although some similarities can be found between curves for muscles like *Deltoideus Anterior*, *Deltoideus Medius*, *Triceps Brachii* (long head), for majorities of muscles the predicted profile deviates considerably from the experimental one. To quantify this difference, the RMSE between experimental and predicted activation was computed for each muscle along with the mean and standard deviation values (Table 8).

Table 8 - RMSE values of the nine muscles. Mean and standard deviation (std) of RMSE values

Muscle	**RMSE**	**Mean $\pm$ Std**
Deltoideus Anterior	0.19085	0.28344 ± 0.17062
Deltoideus Medius	0.13127	
Deltoideus Posterior	0.25575	
Pectoralis Major	0.36255	
Biceps Brachii (long head)	0.39929	
Biceps Brachii (short head)	0.50538	

Brachioradialis	0.17091	
Triceps Brachii (long head)	0.0243	
Triceps Brachii (lateral head)	0.5107	

As it is also possible to verify in the graphs in Figure 24, the results in Table 8 reveal that the estimates of muscle activations of the Biceps Brachii (short head) and Triceps Brachii (lateral head) muscles are the furthest from reality, with a maximum RMSE around 51 %, while the minimum was 2.43 % for *Triceps Brachii* (long head) muscle. Demonstrating overall large differences between the measured activations and the predicted ones by MocoInverse, with a mean RMSE of (28.34 $\pm$ 17.06) %.

Additionally, it was studied the influence on the results when adding experimental EMG tracking to the initial algorithm. The muscle activations were computed with the same model, interval of time, input kinematics and forces files but with inclusion of a cost term for the reference experimental EMG, which involves the preparation of additional input file that contains the experimental measured normalized activations of the nine muscles selected, the solution is then found with the goal of minimizing the differences between predicted and reference activations. The problem was solved in 2 h 43 min with the same CPU, being the resultant muscle activation curves presented in Figure 25, and the respective RMSE values in Table 9.

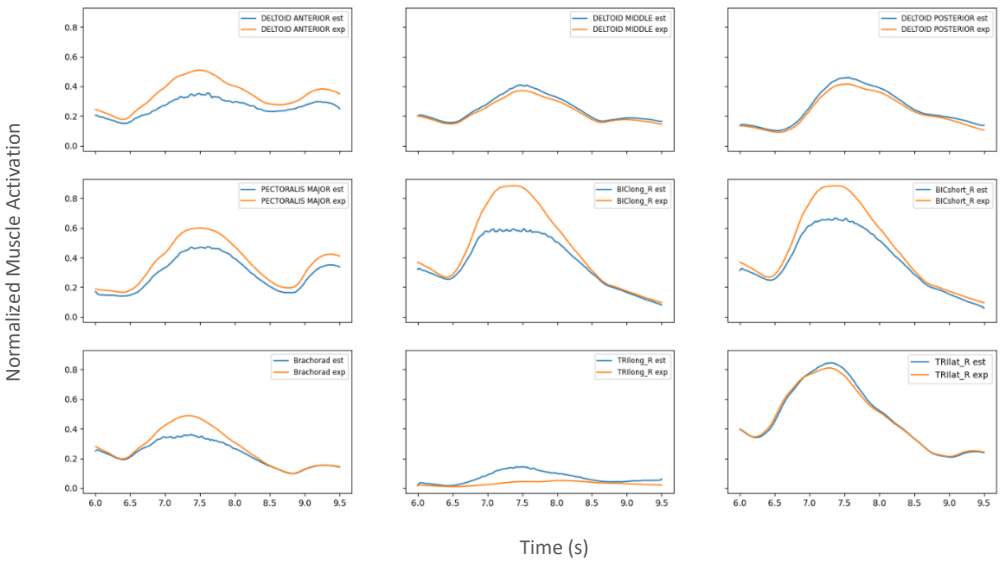

Figure 25 - Normalized experimental (orange) and estimated (blue) muscle activations during execution of maximum isometric force (6.0 s to 9.5 s), obtained by MocoInverse with EMG tracking.

Table 9 - RMSE values of the nine muscles. Mean and standard deviation (std) of RMSE values

Muscle	**RMSE**	**Mean $\pm$ Std**
Deltoideus Anterior	0.09636	0.06599 ± 0.04236
Deltoideus Medius	0.02036	
Deltoideus Posterior	0.02488	
Pectoralis Major	0.07882	
Biceps Brachii (long head)	0.1378	
Biceps Brachii (short head)	0.10828	
Brachioradialis	0.05902	
Triceps Brachii (long head)	0.0497	
Triceps Brachii (lateral head)	0.01869	

Analyzing the graphs of Figure 25, it is possible to verify that predicted activation profile and peak value are closer to the experimental ones, especially for *Triceps Brachii* (lateral head), *Deltoideus Medius* and *Deltoideus Posterior* muscles, as it also possible to confirm trough their RMSE values (Table 9), with errors less than 2.5 %. Conversely to *Biceps Brachii* muscles in which the maximum error is detected with a value of 13.8 %, although the mean error is (6.60 ± 4.24) %. Comparing both raw *MocoInverse* and *MocoInverse* with EMG tracking results it possible to conclude that addition of the experimental activation data to the objective function contributes to a better muscle activation prediction closer to reality, with an error decrease of 23 %. Since the inclusion of EMG tracking contributes to better results, this algorithm was selected as the main solver for the force scaling procedures calculations that comprises muscle redundancy problems.

6.2. Final trials and results

After data processing, the scaling process was then initialized for each of the subjects, starting with geometrical scaling. Utilizing Opensim Scaling tool (Opensim version 4.3), the geometrical upper body model was scaled by introducing the

respective files of markers positions and weights, motion, and total mass value of the scaled model. This last parameter was defined as subject total upper body mass, including the upper extremities, head, torso, and pelvis, and was determined by multiplying subject's total mass by the percentage corresponding to the upper mass of the human body, which was 58.17 % for female and 60.8 % for male [75]. The resultant marker error, root mean square (RMS) error and maximum error, for each scaled model is presented on Table 10.

Table 10 - Marker error after model scaling

Marker error		
RMS error/(cm)		Maximum error/(cm)
Subject 1	1.392	2.877
Subject 2	1.630	2.749
Subject 3	1.404	2.811
Subject 4	1.476	2.741
Subject 5	1.203	1.979

These errors values are slightly above than desired, as Opensim documentation recommends a maximum marker error less than 2 cm for bony landmarks and an RMSE less than 1 cm, which can affect further calculations. These errors values can be due to difference in definitions amid model and subject body marker's locations, choices of scaling factors or scaling markers pairs for each model segment on the scaling tool, IMUs displacement during data collection or electromagnetic interferences that affect the motion tracking accuracy and contribute to deviations from the actual dimensions of the segments and location of anatomical landmarks or joint centers.

Once the geometric scaling process was completed, the calculation of force scaling factors to be applied to each subject´s scaled model was carried out. As

mentioned in Chapter 5, a factor or several factors are calculated by each of the six methods with the aim of adjusting the isometric peak muscle force and thus obtain a strength scaled model. From the first part of the experimental trials, encompassing 15 trials, the data was processed and from the five trials of each joint movement, the one that presented the maximum exerted force value was selected to be used as the basis for the scaling factor calculations (Table 11). From this trial, the kinematics, external loads, torques, and EMG files were formatted according to the Moco Opensim specifications, and subsequently with the addition of the scaled geometrical model, were used as input data to compute muscle activation using MocoInverse with EMG tracking. The reaction force was assumed to be unidirectional (y-axis) and pointing downward (negative), and the resulting torques were calculated by multiplying the force by the distance from the force application point to the elbow or shoulder joint.

Table 11 - Maximum value of force exerted (N) and respective trial for each subject and movement

	Elbow flexion		**Shoulder flexion**		**Shoulder abduction**	
Subject	Trial	Maximum force value/(N)	Trial	Maximum force value/(N)	Trial	Maximum force value/(N)
1	1	111.277	5	53.156	5	44.218
2	5	93.350	5	75.484	5	75.891
3	4	132.523	2	113.234	2	107.606
4	2	191.690	1	131.837	3	135.691
5	4	170.220	2	76.175	1	59.802

Before testing the several force scaling algorithms, the muscle redundancy problem is initially solved with the musculoskeletal model geometrically scaled, but in which a factor is applied to strengthen the model to guarantee the convergence of the solver within the defined tolerance, that is, so that does not occur saturation of muscle recruitment, characterized on the simulation by continuous muscle activation value without variation on response. The strength factor (Table 12) chosen for each subject was defined as the minimum value that ensures the achievement of the optimal solution in any of the three movements.

Table 12 - strength factor selected for each subject

Subject	Strength factor
1	2
2	6
3	5
4	10
5	3

It should be noted that this value is a multiplication factor with respect to the original strength properties of the generic model. Starting by computing the muscle activations with the models already strengthened the several force scaling algorithms were computed and applied to the models, culminating on the calculation of the RMSE between the experimental activations and the ones predicted by the models. The interval of time selected to run the simulation encompassed the period where the peak force was exerted by the subject, being the joint angle value constant and maximum. Residual actuators that account for dynamic discrepancies between the model and the measured motions and forces were added to the model on pelvis body. All simulations were done under the following *MocoInverse* tool settings:

- Solver: “MocoCasADiSolver “
- Maximum iterations number: 1000
- Convergence tolerance: 0.001
- Constraint tolerance: 0.001
- Mesh interval: 0.02

In the case of the optimization-based methods (SS, MS, SM) the muscle activations predicted by the model with only the application of the initial strength factor were used as initial guess to compute the scale factor(s), with the goal of minimizing the differences between experimental and predicted activations. For the multi-objective optimization method (SM) the activations predicted for all the three movements were added to the objective function, meanwhile in the single-objective optimization methods (SS and MS) the calculation of the factor(s) was based on the differences in activations of the movement in which the greatest error was observed, in this case being elbow flexion for subject 1 and shoulder flexion for the others.

The RMSE (mean and standard deviation) values for all six force scaling methods (M, ML, H, SS, SM, MS) and for the model with only the initial strength factor applied (O) are presented on the Tables 13,14 and 15 for each one of the three movements (elbow flexion, shoulder abduction, shoulder flexion). For the optimization-based algorithms (SS, SM, MS) the RMSE is correspondent to the minimum value computed within the ten cycles completed. This number was defined considering the balance between the computer time required to run the algorithm, namely to estimate muscle activation, and finding an optimal solution, i.e., a scaling factor that minimizes the error.

Table 13 - RMSE (mean and standard deviation) values of the scaling methods for elbow flexion

Elbow Flexion							
Subject	**Method**						
1	**O**	**M**	**ML**	**H**	**SS**	**SM**	**MS**

	0.1522 ± 0.0953	0.1129 ± 0.0506	0.0683 ± 0.0405	0.0874 ± 0.0524	0.1098 ± 0.0492	0.0988 ± 0.0618	0.0719 ± 0.0427	**RMSE** (Mean ± Std)
2	0.0292 ± 0.0245	0.0307 ± 0.0254	0.0318 ± 0.0299	0.0287 ± 0.0241	0.0334 ± 0.0269	0.0308 ± 0.0255	0.0463 ± 0.0476	**RMSE** (Mean ± Std)
3	0.0206 ± 0.0213	0.0211 ± 0.0225	0.0183 ± 0.0171	0.0206 ± 0.0211	0.0245 ± 0.0263	0.0205 ± 0.0193	0.0450 ± 0.0650	**RMSE** (Mean ± Std)
4	0.0121 ± 0.0078	0.0121 ± 0.0078	0.0107 ± 0.0059	0.0121 ± 0.0079	0.0123 ± 0.0080	0.0123 ± 0.0082	0.0081 ± 0.0106	**RMSE** (Mean ± Std)
5	0.0659 ± 0.0423	0.0788 ± 0.0524	0.0463 ± 0.0284	0.0535 ± 0.0330	0.0581 ± 0.0362	0.0656 ± 0.0421	0.0751 ± 0.1145	**RMSE** (Mean ± Std)

Table 14 - RMSE (mean and standard deviation) values of the scaling methods for shoulder abduction

Shoulder Abduction							
Subject	**Method**						
1	**O**	**M**	**ML**	**H**	**SS**	**SM**	**MS**

	0.0215 ± 0.0231	0.0263 ± 0.0175	0.0658 ± 0.0482	0.0541 ± 0.0383	0.0198 ± 0.0145	0.0362 ± 0.0261	0.0666 ± 0.0710	**RMSE** (Mean ± Std)
2	0.0888 ± 0.0896	0.0855 ± 0.0879	0.0922 ± 0.0882	0.0898 ± 0.0901	0.0807 ± 0.0856	0.0852 ± 0.0877	0.0976 ± 0.1181	**RMSE** (Mean ± Std)
3	0.0136 ± 0.0086	0.0126 ± 0.0082	0.0154 ± 0.0094	0.0138 ± 0.0087	0.0096 ± 0.0073	0.0142 ± 0.0089	0.0246 ± 0.0316	**RMSE** (Mean ± Std)
4	0.0516 ± 0.0450	0.0516 ± 0.0450	0.0672 ± 0.0688	0.0513 ± 0.0447	0.0505 ± 0.0437	0.0506 ± 0.0413	0.0255 ± 0.0329	**RMSE** (Mean ± Std)
5	0.0231 ± 0.0203	0.0263 ± 0.0243	0.0193 ± 0.0154	0.0201 ± 0.0164	0.0212 ± 0.0179	0.0207 ± 0.0183	0.0167 ± 0.0121	**RMSE** (Mean ± Std)

Table 15 - RMSE (mean and standard deviation) values of the scaling methods for shoulder flexion

Shoulder Flexion							
Subject	**Method**						
1	**O**	**M**	**ML**	**H**	**SS**	**SM**	**MS**

	0.0644 ± 0.0463	0.0351 ± 0.0239	0.1259 ± 0.1045	0.0896 ± 0.0699	0.0397 ± 0.0265	0.0603 ± 0.0434	0.0544 ± 0.0377	**RMSE** (Mean ± Std)
2	0.2391 ± 0.1555	0.2048 ± 0.1339	0.2780 ± 0.1745	0.2523 ± 0.1658	0.1551 ± 0.1219	0.2014 ± 0.1322	0.2274 ± 0.1503	**RMSE** (Mean ± Std)
3	0.1331 ± 0.1528	0.1187 ± 0.1364	0.1667 ± 0.1947	0.1350 ± 0.1550	0.0687 ± 0.0746	0.1405 ± 0.1613	0.0245 ± 0.0645	**RMSE** (Mean ± Std)
4	0.1733 ± 0.1111	0.1733 ± 0.1111	0.1600 ± 0.1570	0.1714 ± 0.1097	0.1648 ± 0.1448	0.1641 ± 0.1441	0.1071 ± 0.1031	**RMSE** (Mean ± Std)
5	0.1706 ± 0.0744	0.1474 ± 0.0713	0.2112 ± 0.1174	0.2081 ± 0.1092	0.1925 ± 0.0918	0.1713 ± 0.0748	0.0542 ± 0.0694	**RMSE** (Mean ± Std)

Observing the results, it can be seen some variations on the RMSE between methods that may contribute unfavorably or favorably when compared to error that does not involve its application (O). Among them, the greater variations were reached by method MS and SS on the shoulder flexion, as well for method ML, though the error is greater. In relation to methods M and H, with respect to subjects 2, 3, and 4 there are situations in which the value is equivalent to the initial error value (O), which is

likely, because the mass and the height values of the generic model are nearly the same to those of these subjects, resulting in a scale factor of approximately the value one, which does not occur in subjects 1 and 5 who have notably different body properties. Method SM also does not influence the error remarkably, as it tries to minimize the differences of the activations between the three movements.

To assess the influence on the initial error value (O) of the presented six methods (M, ML, H, SS, SM, MS), a one-tailed paired samples test was carried out with the null hypotheses that the mean difference between the pair is equal or greater than zero. First, the assumptions of the parametric paired samples t-test for each pair were evaluated: (1) the differences between the two set of values are independent of one another; (2) The differences between the matched pairs should be approximately normally distributed; (3) No outliers in the differences between the two groups. This analysis was executed for each of the three movements.

Assured the independence of the subjects and measurements, the normality was assessed through Shapiro-Wilk test for each pair, being the results presented in Table 16.

Table 16 - The p-values of the normality tests for all pairs (M-O, ML-O, H-O, SS-O, MS-O, SM-O) respective to the motion (Elbow flexion, Shoulder flexion, Shoulder abduction), considering a significance level of 5 %. The significant values (p-value < 0.05) appear in bold

Test of Normality (Shapiro-Wilk)					
Elbow flexion		Shoulder flexion		Shoulder abduction	
	p		p		p
M-O	**0.046**	M-O	0.747	M-O	0.849
ML-O	**0.019**	ML-O	0.333	ML-O	0.164
H-O	**0.005**	H-O	0.708	H-O	**0.002**
SS-O	**0.024**	SS-O	0.867	SS-O	0.121
MS-O	**0.048**	MS-O	0.205	MS-O	0.852
SM-O	**< 0.001**	SM-O	0.245	SM-O	**0.029**

The assumption of normality is violated by all the groups in elbow flexion and H-O, SM-O groups in shoulder abduction, the remaining pairs didn´t show a significant difference ($p<0.05$) suggesting that the pairwise differences are normally distributed.

For these pairs, then existence of outliers between its differences was analysed trough boxplots.

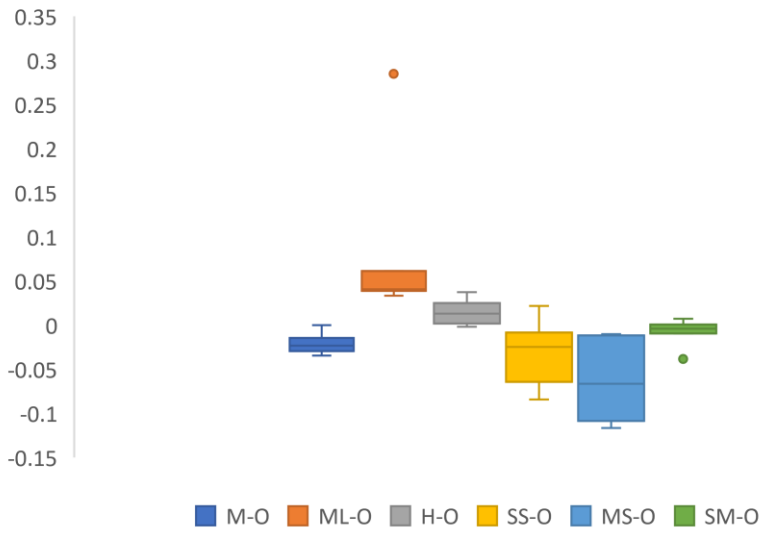

Figure 26 - Boxplots for M-O, ML-O, H-O, SS-O, MS-O, SM-O in shoulder flexion.

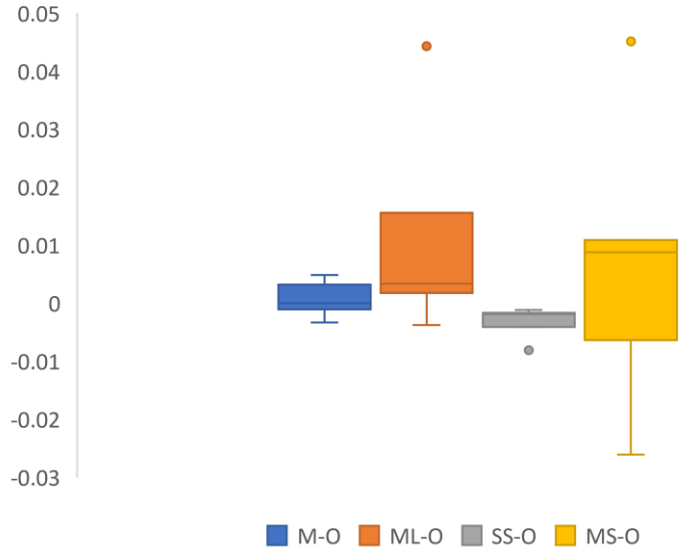

Figure 27 - Boxplots for M-O, ML-O, H-O, SS-O, MS-O, SM-O in shoulder abduction.

In case of shoulder flexion (Figure 26), It is verified the existence of outliers in SM-O and ML-O groups, and in ML-O, SS-O, MS-O in shoulder abduction (Figure 27)

violating the assumption of inexistence of outliers. For these variables an equivalent non-parametric test was selected, the Wilcoxon's signed rank test, for the other pairs that passed all assumptions a paired samples t-test was carried out.

Starting by elbow flexion, based on the results of Table 17 no statistically significant differences were verified, since the p-value for all pairs was greater than the significance level of 5 %, failing to reject the null hypothesis. The median differences between pairs, represented by Hodges-Lehmann Estimate, are minimal, thus concluding the methods M, ML, H, SS, MS, SM had no significative effect on the initial error value for elbow flexion.

Table 17 - Wilcoxon signed rank test for all pairs in elbow flexion, considering a significance level of 5 %

	W	p	Hodges-Lehmann Estimate
M-O	6	0.708	< 0.001
ML-O	3	0.156	-0.011
H-O	2	0.094	-0.006
SS-O	6	0.406	-0.002
MS-O	9	0.688	0.007
SM-O	6	0.406	> -0.001

Regarding shoulder abduction, in Table 18 and Table 19 only SS-O demonstrated significant results (p-value =0.031), while the other variables failed to reject null hypothesis.

Table 18 - Paired samples t-test for group M-O in shoulder abduction, considering a significance level of 5 %

	t	df	p	Mean Difference	SE Difference
M-O	0.484	4	0.673	7.118×10^{-4}	0.001

Table 19 - Wilcoxon signed rank test for ML-O, H-O, SS-O, MS-O, SM-O variables in shoulder abduction, considering a significance level of 5 %. The significant values (p-value < 0.05) appear in bold

	W	p	Hodges-Lehmann Estimate
ML-O	12	0.906	0.009
H-O	9	0.688	< 0.001
SS-O	0	**0.031**	-0.003
MS-O	10	0.781	0.009
SM-O	6	0.406	< 0.001

Lastly, in both tests (Table 20 and 21) performed for shoulder flexion only groups M-O and MS-O showed significant results, with a respective p-value of 0.014 and 0.026.

Table 20 - Paired samples t-test for M-O, H-O, SS-O, MS-O in shoulder abduction, considering a significance level of 5 %. The significant values (p-value < 0.05) appear in bold

	t	df	p	Mean Difference	SE Difference
M-O	-3.346	4	**0.014**	-0.02	0.006
H-O	2.072	4	0.946	0.015	0.007
SS-O	-1.677	4	0.084	-0.032	0.019
MS-O	-2.748	4	**0.026**	-0.063	0.023

Table 21 - Wilcoxon signed rank test for ML-O, SM-O variables in shoulder abduction, considering a significance level of 5 %

	W	p	Hodges-Lehmann Estimate
ML-O	14	0.969	0.037
SM-O	4	0.219	-0.004

As described, out of the six force scaling methods only M, MS, SS presented significative results with a p-value of 0.014, 0.026 in shoulder flexion and 0.031 in shoulder abduction respectively. Out of the optimization-based methods with single

objective (MS and SS), only method MS had a notable influence on minimizing shoulder flexion error, although the SS-O pair also showed a negative mean difference, this was not found to be statistically significant. In addition, the factor obtained by the SS method promoted a significant reduction in the shoulder abduction error, despite this motion was not considered in the objective function, which may arise from the similarity in muscle recruitment of shoulder flexion and abduction, namely the deltoid muscle. In MS method this was not verified as a different factor is obtained for each muscle with the goal of minimizing the muscle activation specific to that motion. For the remaining approaches, except for the body mass-based method (M) that promoted a better fit to the experimental activations in shoulder flexion, the calculated scaling factors either had no effect or contributed to maximizing the error of the simulation results.

To test the influence of the force scaling process in simulation prediction, using the data collected from part II of the protocol corresponding to point-to-point exercises, the muscle activation was estimated and further compared to the associated experimental activations. The RMSE was computed for the same models with initial scale factor (O) and after force scaling with approaches MS, SS. These two approaches were chosen to study the effect of applying a unique scale factor, equal for all muscles (method SS) or a specific factor associated to each muscle (method MS). The RMSE values (mean and standard deviation) for each approach are shown in Table 22.

Table 22 - RMSE (mean and standard deviation) values of the scaling methods for point-to-point exercises

Subject	**Method**			
1	O	SS	MS	
	0.0149 $\pm$ 0.0006	0.0158 $\pm$ 0.0003	0.0238 $\pm$ 0.0016	**RMSE** (Mean $\pm$ Std)

2	0.0167 ± 0.0030	0.0201 ± 0.0027	0.0281 ± 0.0006	**RMSE** (Mean ± Std)
3	0.0157 ± 0.0087	0.0160 ± 0.0083	0.0176 ± 0.0057	**RMSE** (Mean ± Std)
4	0.0301 ± 0.0053	0.0297 ± 0.0050	0.0087 ± 0.0003	**RMSE** (Mean ± Std)
5	0.0438 ± 0.0079	0.1146 ± 0.0692	0.0570 ± 0.0272	**RMSE** (Mean ± Std)

The greatest variations, with positive or negative differences relative to O are registered in the MS method for subjects 2, 4 and 5, while for SS method there are no notable changes, apart from subject 5. A two-tailed paired samples t-test was carried out to study the effect of the force scaling methods on simulation results, namely muscle activation. The assumptions for a parametric paired samples t-test of independence, normality and existence of outliers were evaluated for each group. The normality of the groups (MS-O, SS-O) was assessed trough Shapiro-Wilk test for each pair, being the results presented in Table 23.

Table 23 - The p-values of the normality tests for pairs (SS-O, MS-O) considering a significance level of 5 %. The significant values (p-value < 0.05)

Test of Normality (Shapiro-Wilk)		
	W	p
SS-O	0.592	**< 0.001**

MS-O	0.796	0.075

Significative differences (p <0.05) were found for pair SS-O, suggesting that the pairwise differences are not normally distributed. Checked this assumption, next the existence of outliers was examined for group MS-O (Figure 28) , with one outlier being found implying the normality of this group.

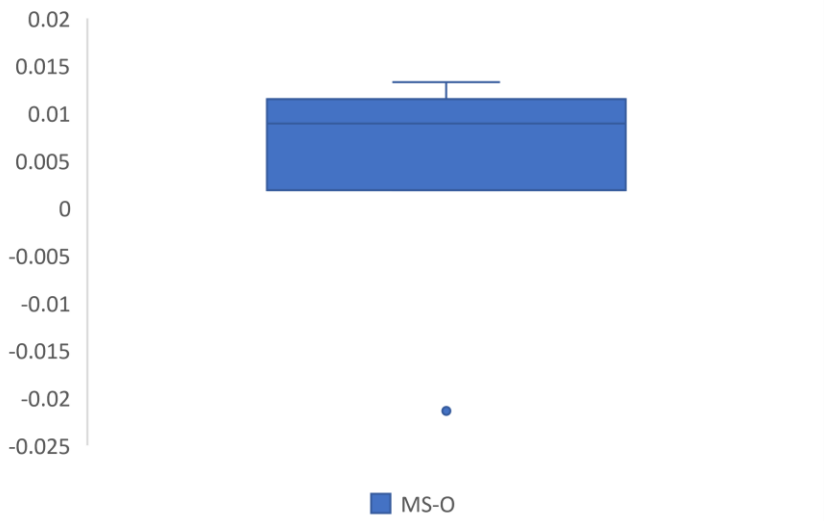

Figure 28 - Boxplot for variable MS-O.

Failing the approval of the assumptions the pairwise differences were assessed trough Wilcoxon ´s signed rank test, presented on Table 24.

Table 24 - Wilcoxon signed rank test for SS-O, MS-O, considering a significance level of 5 %

	W	p	Hodges-Lehmann Estimate
SS-O	13	0.188	0.002
MS-O	10	0.625	0.007

No significative differences were found for both groups, thus concluding that none of the methods contributed to remarkably change the initial error. The Figure 29 and

Table 25 shows the boxplot and descriptive statistics for the variables O, SS and MS, the variable O has the lowest median line between the three variables with a value lower than 0.02 which means half of the error values are greater than or equal to this value and half are less. Method SS shows a lower median than method MS, so on average its error value is lower. Both variables have outliers, with MS having a lower data dispersion than SS, with the lowest interquartile range (IQR) between the three methods, suggesting less variability in the middle 50 % of the data.

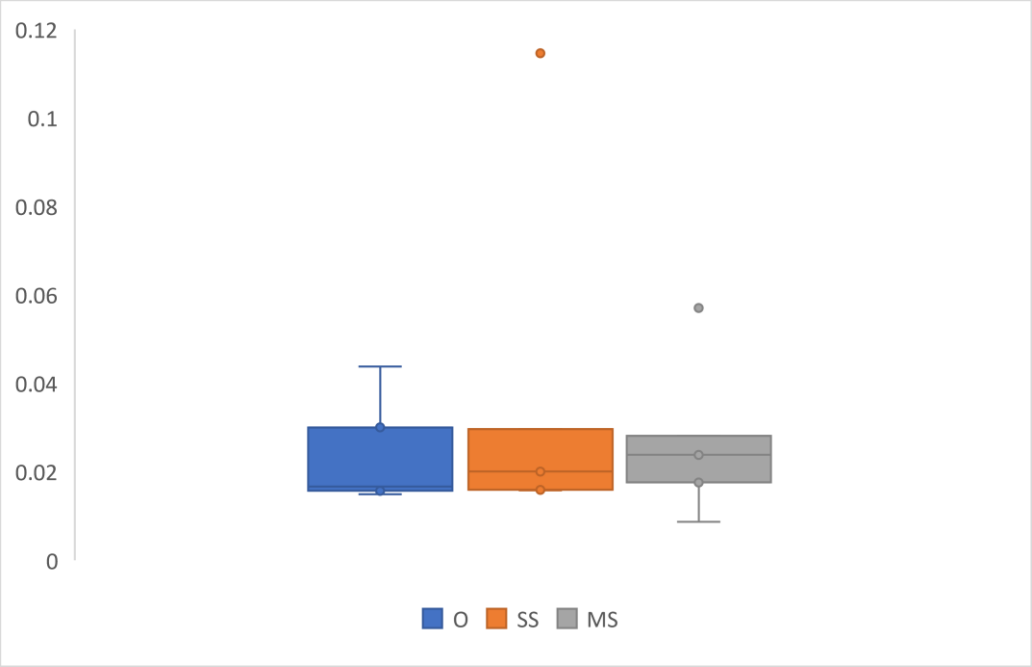

Figure 29 - Boxplots for variables O, SS and MS in point-to-point exercises.

Table 25 - Descriptive statistics for variable O, S, MS

	O	SS	MS
Median	0.017	0.02	0.024
Mean	0.024	0.039	0.027
Minimum	0.015	0.016	0.009
Maximum	0.044	0.115	0.057
Range	0.029	0.099	0.048

IQR	0.014332	0.013728	0.01055

Thus, it can be concluded that the force scaling methods did not have the ability to influence the results, in this case the estimation of muscle activation, with the best results being achieved with the initial model that was primarily uniformly scaled with a factor. The outlier in the SS group is consequence of the no convergence of the solver in two of point-to-point trials computed for that subject, resulting in an extreme error value. In MS method, a different factor is obtained for each muscle, which may lead to larger force discrepancies between muscle groups, contributing to a greater error.

To further explore the application of a force scale factor to the geometric scaled model and its impact on muscle activation prediction accuracy by *MocoInverse* tool with EMG tracking, a scatter plot of the scale factor versus the mean RMSE of muscle activations was traced (Figure 29), for one of the subjects (subject 2). Using the same subject´s model, the activation error was calculated for two movements, shoulder flexion and point-to-point, while increasing the factor from two to fourteen. These factors are multiples of the initial force proprieties of the generic model, i.e, the peak isometric muscle force.

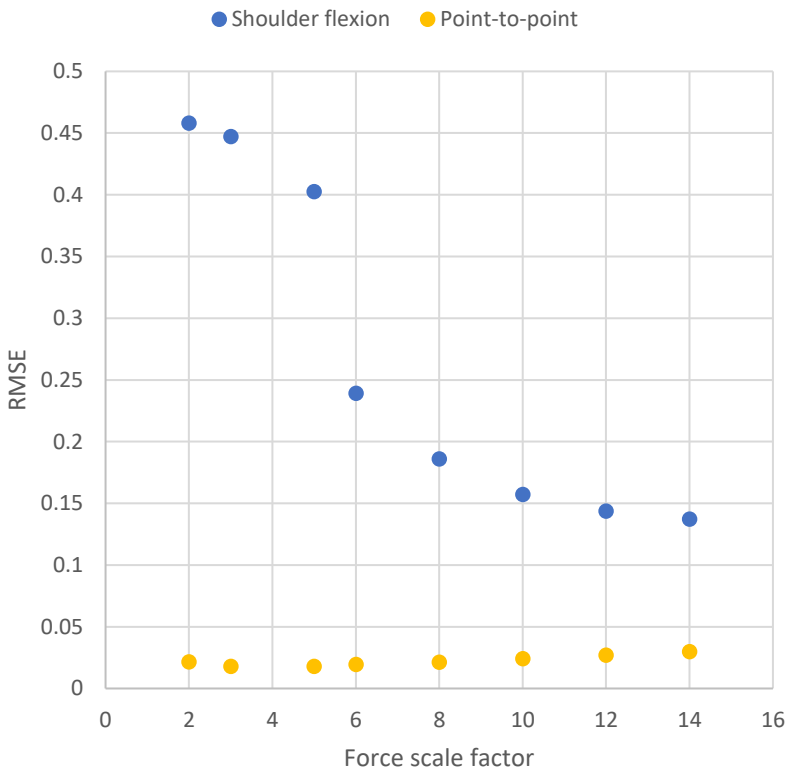

Figure 30 - Scatter plot of the scale factor versus the mean RMSE of muscle activations, for shoulder flexion and point-to-point exercises.

As shown in the plot, for the shoulder flexion motion in blue, as the scale factor increases, the error decreases abruptly until it stabilizes, resembling a parabolic profile. Contrary to point-to-point movement, where there is a subtle increase in error as you move along the x-axis, but never reaching 5%. For shoulder flexion, smaller factors result in RMSE values greater than 40%, which represents poor tracking of experimental activation. From factor six onwards the error decreases from 24% to a minimum of 14% and a change in curvature shape occurs. Thus, although the force scaling factor strongly influences the tool tracking accuracy for shoulder flexion, the same is not true for the point-to-point exercise, which was a much smaller error. The greater error in shoulder flexion may be due to uncertainties of the input data like joint angles or external loads, as well the short time the simulation was run over. While, for to point-to-point exercises where the 30 s movement was fully evaluated, for shoulder flexion only the short period of 5 s was evaluated, which comprises only the period of application of maximum isometric force, translated initially by a sudden

increase in muscle activation, which may lead to less robustness of the initial guess and following calculations. Changes on net joint moments faster than allowed by deactivation and activation time constants may also compromise the result [76]. Isometric shoulder flexion involves the development of higher forces and moments, errors in measurements of these quantities as well as joint angles, plus motion´s noise and unrealistic accelerations or net joint moments contribute strongly to lower accuracy of simulation estimates [5,76]. Compared to isometric shoulder flexion, in which there is a force opposing the movement and holding the joint in position, resulting in an effort situation with continuous increase in the activation level closer to maximum value, the point-to-point exercise is only subjected to body weight and full mobility of the shoulder and elbow joint is allowed, showing lower muscle activation levels without sudden changes.

Since the initial scale factor was obtained over the period when the peak isometric force was exerted, a correlation analysis was performed to investigate the possibility of a linear association amid these variables, the maximum force exerted in the isometric exercises and the initial strength scaling factor applied to the model post geometrical scaling. The values selected for maximum force were respective to shoulder flexion motion, since it was the movement most sensitive to factor change and the most prone to the optimal solution not being found. The assumptions of normality, linearity and outliers for parametric correlation analysis were verified. The Shapiro-Wilk test in Table 26 demonstrated no significative results ($p<0.05$), suggesting that both variables are approximately normally distributed.

Table 26 - The p-values of the normality tests for variables Maxforce (Maximum force) and Sfactor (Scale factor), considering a significance level of 5 %

Test of Normality (Shapiro-Wilk)		
	W	p
Maxforce	0.923	0.551
Sfactor	0.941	0.67

The scatterplot (Figure 31) of one variable against the other displayed a linear relationship, as well no outliers were found in the boxplot of both variables (Fig. 31), so none of the main assumptions were violated.

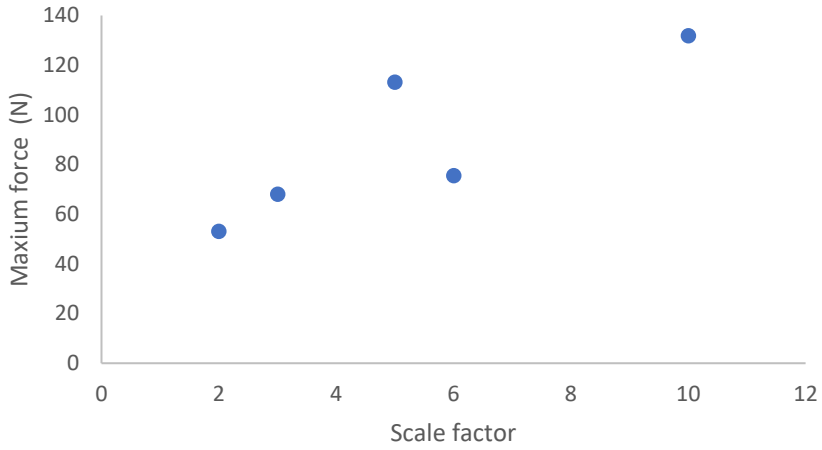

Figure 31 - Scatterplot of Scale factor and Maximum force (N).

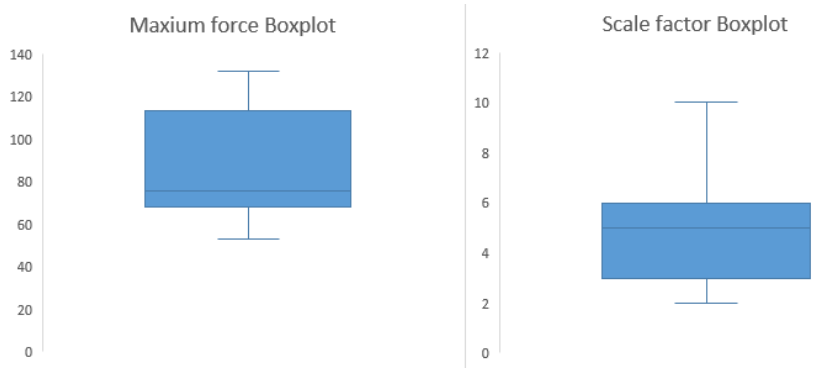

Figure 32 - Boxplots for variables Maximum force (Left) and Scale factor (Right).

Pearson's correlation test was then run, testing the null hypothesis that there is no association between the two variables. The resultant Pearson's r value and p value are shown on Table 27.

Table 27- Pearson’s r and p values for Maxforce-Sfactor pair

Pearson's Correlations		
	Pearson's r	p
Maxforce-Sfactor	0.856	0.064

The results reveal a strong, positive correlation (r=0.856) between maximum force exerted in shoulder flexion and the strength scale factor applied to the model, however not statistically significant (p = 0.064 >0.05), concluding that there is no significant linear association between the variables. So, although may exist a correlation between variables in the sample (n=5), it cannot be extrapolated to the population, requiring a larger sample size to test this hypothesis.

7. Conclusions and Future work

This dissertation was developed with the foundation of creating a highly user-specific upper limb model, englobing the process of transforming a generic model into a scaled-generic model, with focus on the understudied field of upper limb model´s force scaling. The scaling of model´s strength proprieties was addressed through several methods and its impact on simulation outputs was validated against experimental data.

In Chapter 4, a review concerning Opensim error, user-specific scaling, geometrical and force scaling approaches was conducted. From modeling variables to input parameters, the main sources of error in Opensim simulations, as well as its quantification, were identified and noted for the upcoming calculations. After considering the study conditions, the use of scaled-generic models was selected, and their scaling process was addressed. The importance and impact of geometrical scaling

on simulation results was highlighted, as well as an analysis of the main advantages and disadvantages of the different approaches that can be used in this scaling procedure. Lastly, a review of force scaling methods was held, which proved to be scarce for upper limb models, nevertheless it was possible to identify the fundamentals of the various methodologies and divide them into two main groups: mass-length, muscle volume-based and moment-based methods.

Chapter 5 aborded the methodology used in this thesis to convert a generic model to a user-specific model. The conversion process is initiated by scaling of the geometrical proprieties using Opensim scale tool by input of body mass, markers 3D coordinates and definitions of the scale factors that will scale each body segment. Next, it was described the procedure to adjust the peak isometric force of the model, which was defined as the product between the generic muscle isometric force and a scale factor. To obtain this factor, six different approaches were introduced, including those discussed in Chapter 4, in addition to the optimization algorithms designed based on muscle activation. In the latter, the scaling factor was determined by running several cycles, starting with the prediction of muscle activation by *MocoInverse* and culminating in the attainment of the force scaled model.

From Chapter 6 onwards, the experimental tests performed to validate the methods covered in the methodology (Chapter 5), as well as their respective results, were described. Two types of exercises were executed, and respective data was collected, in order to use as input to the biomechanical simulations, with the goal of obtaining muscle activation. Muscle activations were predicted using the *MocoInverse* tool with associated EMG tracking, as pre-tests revealed greater accuracy with this addition than using the tool alone. For each of the three isometric movements (elbow flexion, shoulder flexion, shoulder abduction), the average RMSE between estimated and experimental activations of nine muscles was calculated for each model scaled by each of the six methods. From these results it was possible to conclude that none of the methods contributed to minimize the error for all three motions simultaneously, which was expected for the methods based on single-objective optimization (SS and MS), since the factor is obtained by minimizing the activation differences with respect to one of the motions, namely the one with the highest RMSE value for the model with

only the application of an initial force factor that allows the solver to converge. Out of all force scaling approaches, only M, MS and SS showed significant results that favored better accuracy of the results for one of the three motions. The same metrics, muscle activation and RMSE, were estimated and calculated for models scaled by the MS and SS method but using a point-to-point exercise as the input kinematics. Statistical analysis of the results revealed that neither approach contributes to significantly decrease the error relative to that obtained by the scaled model with the initial scale factor. Furthermore, to study the influence of the scaling of model´s force properties on the muscular activation prediction, a scatter plot of the RMSE versus the initial scaling factor, expressed by an integer, was generated for one of the subjects in the conditions of shoulder flexion and point-to-point movements. The graph demonstrated different variations for each motion, with shoulder flexion being the most affected by the change of the scale factor, translated by an inverse relationship, where the increase of the scale factor value tends to drastically reduce the error, ranging from values of 46 % to 14 %. The same effect was not observed for the point-to-point movement, with a slight increase in the error, although not more than 5 %. The greater error in shoulder flexion may result from uncertainties in the input joint angles and the time interval analyzed, which presents a rapid and increasing variation of the muscle activation profile. The different effect of the scaling factor between movements is probably due to the existence of an opposing force equivalent in magnitude to the net force exerted by the subject, which is one of the simulation inputs, unlike the point-to-point movement where external forces other than gravity were not applied. Since the *MocoInverse* tool solves the muscle redundancy problem based on the kinematics that is prescribed, uncertainties in the motion, external forces and moments strongly affect the accuracy of the results. Another factor with influence on the simulation results are the settings of the optimization problem, such as mesh interval, convergence tolerance, constraint tolerance, activation dynamics and tendon compliance, among others, and whose effect was not studied in this thesis. Lastly a correlation between maximum net force applied in shoulder flexion and the force scale factor was examined, being the factors positive integer numbers. It was concluded that although may exist a positive correlation it is not significant, needing an evaluation with a larger sample size.

Thus, it can be concluded that the scaling of the force properties of the model has a more significant influence on the simulation results in situations involving the development of forces and moments of greater module, having a noticeable impact on finding the optimal solution, in this case muscle activation. Not undervaluing, however, the strong effect of the inputs kinematics and problem settings on the accuracy of the results. One of the main limitations of this work is the small number of samples that may have led to inconclusive results. The choice of the point-to-point exercise to validate the force scaling methods may not have been the most adequate since the activation levels only reached average values. The force scaling methods investigated in this work were applied to the model after pre-scaling, not being studied concretely a procedure to guarantee the convergence of the solver. The optimization methods developed may be the most suitable for this purpose, however they are time consuming and not directly applicable, requiring several input data, such as EMG. Also, the methods developed did not account for the force variability between right-left upper limb.

For future research, it is proposed to analyze the force scaling approaches for a larger sample and for diversified movements and conditions, such as those conducive to the development of fatigue. Furthermore, using musculoskeletal models and Opensim Moco software, develop a strategy based on the prediction of muscle strength and/or muscle activation, capable of assessing muscle fatigue in a work environment.

References

[1] Gallagher, S., Schall Jr., M. C. (2016). Musculoskeletal disorders as a fatigue failure process: evidence, implications and research needs. DOI: 10.1080/00140139.2016.1208848

[2] Introduction to work-related musculoskeletal disorders How to tackle MSDs?. European Agency for Safety and Health at Work. https://osha.europa.eu/en/publications/factsheet-71-introduction-work-related-musculoskeletal-disorders

[3] Daneshmandi, H., Choobineh, AR., Ghaem, H., Alhamd, M. W., Fakherpour, A. (2017). The effect of musculoskeletal problems on fatigue and productivity of office personnel: a cross-sectional study. Research Center for Health Sciences, Institute of Health, Shiraz University of Medical Sciences, Shiraz, Iran. Journal of Preventive Medicine and Hygiene 58(3): E252-E258.

[4] Al-Mulla, M. R., Sepulveda, F., Colley, M. (2011). A review of non-invasive techniques to detect and predict localized muscle fatigue. Sensors, 11(4), 3545–3594. https://doi.org/10.3390/s110403545

[5] Hicks, J. L., Uchida, T. K., Seth, A., Rajagopal, A., Delp, S. L. (2015). Is My Model Good Enough? Best Practices for Verification and Validation of Musculoskeletal Models and Simulations of Movement. Journal of Biomechanical Engineering, 2015 Feb, 137(2): 020905. Doi: 10.1115/1.4029304.

[6] Musculoskeletal disorders and psychosocial risk factors in the workplace-statistical analysis of EU-wide survey data Executive Summary European Agency for Safety and Health at Work. https://osha.europa.eu/en/publications/executive-summary-musculoskeletal-disorders-and-psychosocial-risk-factors-workplace-statistical-analysis-eu-wide-survey-data

[7] Middlesworth, M. The Definition and Causes of Musculoskeletal Disorders. https://ergo-plus.com/musculoskeletal-disorders-msd/

[8] Work-related Musculoskeletal Disorders (WMSDs) - Risk Factors. 1997-2022 Canadian Centre for Occupational Health & Safety (ccohs). https://www.ccohs.ca/oshanswers/ergonomics/risk.html

[9] Seth, A., Sherman, M., Reinbolt, J., Delp, S. L. (2011). OpenSim: a musculoskeletal modeling and simulation framework for in silico investigations and exchange. 2, 212–232. doi: 10.1016/j.piutam.2011.04.021

[10] Yang, C., Leitkam, S., Coté, J. N. (2019). Effects of different fatigue locations on upper body kinematics and inter-joint coordination in a repetitive pointing task. PLoS ONE, 14(12). https://doi.org/10.1371/journal.pone.0227247

[11] Heeransh, D. D., Shook, M., Varacallo, M. (2021). Anatomy, Skeletal Muscle. https://www.ncbi.nlm.nih.gov/books/NBK537236/

[12] Frontera, W. R., Ochala, J. (2015). Skeletal Muscle: A Brief Review of Structure and Function. In Behavior Genetics (Vol. 45, Issue 2, pp. 183–195). Springer New York LLC. https://doi.org/10.1007/s00223-014-9915-y

[13] Roberts, T. J., Eng, C. M., Sleboda, D. A., Holt, N. C., Brainerd, E. L., Stover, K. K., Marsh, R. L., & Azizi, E. (2019). The multi-scale, three-dimensional nature of skeletal muscle contraction.

In Physiology (Vol. 34, Issue 6, pp. 402–408). American Physiological Society. https://doi.org/10.1152/physiol.00023.2019

[14] Uchida, T. K., Delp, S. L. Biomechanics of Movement: The Science of Sports, Robotics, and Rehabilitation. Cambridge, MA: The MIT Press, 2020. https://simtk-confluence-homeworks.stanford.edu:8443/display/BMH/Lectures

[15] LibreTexts™ Medicine. (2023, January 17). 9.3E: Types of Muscle Contractions: Isotonic and Isometric. https://med.libretexts.org/Bookshelves/Anatomy_and_Physiology/Anatomy_and_Physiology_%28Boundless%29/9%3A_Muscular_System/9.3%3A_Control_of_Muscle_Tension/9.3E%3A_Types_of_Muscle_Contractions%3A_Isotonic_and_Isometric

[16] Fitts; R. H., McDonald; K. S., Schluter, J. M. (1991). The determinants of skeletal muscle force and power: Their adaptability with changes in activity pattern. 24(supp-S1), 111–122. doi:10.1016/0021-9290(91)90382-w

[17] Wan, J. J., Qin, Z., Wang, P. Y., Sun, Y., Liu, X. (2017). Muscle fatigue: General understanding and treatment. In Experimental and Molecular Medicine (Vol. 49, Issue 10). Nature Publishing Group. https://doi.org/10.1038/emm.2017.194

[18] Sa-ngiamsak, T. Assessment of Muscle Fatigue in Work Related Musculoskeletal disorders by High-Density Surface Electromyography. Uporto, University of Porto.

[19] Ortega-Auriol, P. A., Besier, T. F., Byblow, W. D., McMorland, A. J. C. (2018). Fatigue Influences the Recruitment, but Not Structure, of Muscle Synergies. Frontiers in Human Neuroscience, 12. doi:10.3389/fnhum.2018.00217

[20] Gerdle, B., Larsson, B., Karlsson, S. (2000). Criterion validation of surface EMG variables as fatigue indicators using peak torque: a study of repetitive maximum isokinetic knee extensions. 10(4), 0–232. doi:10.1016/s1050-6411(00)00011-0

[21] Muramatsu, Y., Kobayashi, H (2013). Assessment of Local Muscle Fatigue by NIRS. Tokyo, Tokyo University of Science. 2013 Seventh International Conference on Sensing Technology.

[22] Barstow, T. J. (2019). CORP: Understanding near infrared spectroscopy (NIRS) and its application to skeletal muscle research. Journal of Applied Physiology, japplphysiol.00166.2018–. doi:10.1152/japplphysiol.00166.2018

[23] Bartuzi, P., Roman-Liu, D., Wiśniewski, T. (2012). The influence of fatigue on muscle temperature. International Journal of Occupational Safety and Ergonomics, 18(2), 233–243. https://doi.org/10.1080/10803548.2012.11076931

[24] Hadžić, V., Širok, B., Malneršič, A., & Čoh, M. (2019). Can infrared thermography be used to monitor fatigue during exercise? A case study. Journal of Sport and Health Science, 8(1), 89–92. https://doi.org/10.1016/j.jshs.2015.08.002

[25] Mihai, T. (2003). Mechanomyography versus Electromyography, in monitoring the muscular fatigue. 2(1), 3–. doi:10.1186/1475-925x-2-3

[26] Talib, I., Sundaraj, K., Kiang, C., Sundaraj, S. (2018). A systematic review of muscle activity assessment of the biceps brachii muscle using mechanomyography. JMNI, Journal of Musculoskeletal and Neuronal Interactions (Vol. 18, Issue 4).

[27] Musculoskeletal modelling. https://www.imperial.ac.uk/structural-biomechanics/Projects/msk-modelling/

[28] Tutorial 1 - Intro to Musculoskeletal Modeling. https://simtk-confluence.stanford.edu:8443/display/OpenSim/Tutorial+1+-+Intro+to+Musculoskeletal+Modeling

[29] Millard, M., Uchida, T., Seth, A., Delp, S. L. (2013). Flexing computational muscle: Modeling and simulation of musculotendon dynamics. Journal of Biomechanical Engineering, 135(2). https://doi.org/10.1115/1.4023390

[30] Falisse, A., Rossom, S., Jonkers, I., Groote, F. (2017). EMG-Driven Optimal Estimation of Subject-SPECIFIC Hill Model Muscle-Tendon Parameters of the Knee Joint Actuators. IEEE Transactions on Biomedical Engineering, 64(9), 2253–2262. https://doi.org/10.1109/TBME.2016.2630009

[31] Thelen, D. G. (2003). Adjustment of muscle mechanics model parameters to simulate dynamic contractions in older adults. Journal of Biomechanical Engineering, 125(1), 70–77. https://doi.org/10.1115/1.1531112

[32] Delp, S., Hicks, J. (2011). OpenSim Workshop Agenda Day One. https://simtk.org/docman/view.php/611/1567/AdvancedUserWorkshop_Handout.pdf

[33] Muscle Editor. https://simtk-confluence.stanford.edu:8443/display/OpenSim/Muscle+Editor

[34] Overview of OpenSim Workflows.https://simtk-confluence.stanford.edu:8443/display/OpenSim/Overview+of+OpenSim+Workflows

[35] MVN User Manual. Document MVNManual, Revision Z, 01 04 2021.Xsens.

[36] Roetenberg, D., Luinge, H., Slycke, P. (2009). Xsens MVN: Full 6DOF human motion tracking using miniature inertial sensors. Xsens Motion Technol. BV Tech. Rep.. 3.

[37] MVN Biomechanical Model. https://xsenstechnologies.force.com/knowledgebase/s/article/MVN-Biomechanical-Model-1605783181874?language=en_US

[38] Sweet, M., Fracisco, P. Comparing Knee Angle for Subject IMU Self-Placement. https://simtk-confluence.stanford.edu:8443/display/OpenSim/Comparing+Knee+Angle+for+Subject+IMU+Self+Placement

[39] Hsiao, R., Fanton, M. Accurate orientation estimation of the head/neck using inertial measurements units. https://simtk-confluence.stanford.edu:8443/pages/viewpage.action?pageId=21006395

[40] Holzbaur, K. R. S., Murray, W. M., Delp, S. L. (2005). A model of the upper extremity for simulating musculoskeletal surgery and analyzing neuromuscular control. Annals of Biomedical Engineering, 33(6), 829–840. https://doi.org/10.1007/s10439-005-3320-7

[41] Bruno, A. G., Bouxsein, M. L., & Anderson, D. E. (2015). Development and validation of a musculoskeletal model of the fully articulated thoracolumbar spine and rib cage. Journal of Biomechanical Engineering, 137(8). https://doi.org/10.1115/1.4030408

[42] Dembia, C. L., Bianco, N. A., Falisse, A., Hicks, J. L., Delp, S. L. (2020). OpenSim Moco: Musculoskeletal optimal control. Computational Biology, 12 December. https://doi.org/10.1371/journal.pcbi.1008493

[43] Lewandowski, B., Pennline, J, Thompson, B., Humphreys, B., Ryder, J, Ploutz-Snyder, P, Mulugeta, L (2014). Uncertainty, Validation and Sensitivity Analyses of the OpenSim Muscle Model for Pre- and Post-flight Strength Predictions. NASA Human Research Program, Investigators' Workshop, February 12-13, 2014. https://ntrs.nasa.gov/api/citations/20140005392/downloads/20140005392.pdf

[44] Trinler, U., Leboeuf, F., Hollands, K., Jones, R.; Baker, R. (2018). Estimation of muscle activation during different walking speeds with two mathematical approaches compared to surface EMG. Gait and Posture 64, 266–273. https://doi.org/10.1016/j.gaitpost.2018.06.115

[45] Montefiori, E., Fiifi Hayford, C., Mazzà, C. (2022). Variations of lower-limb joint kinematics associated with the use of different ankle joint models. Journal of Biomechanics,136. https://doi.org/10.1016/j.jbiomech.2022.111072

[46] Roelker, S. A., Caruthers, E. J., Baker, R. K., Pelz, N. C., Chaudhari, A. M. W., Siston, R. A. (2017). Interpreting Musculoskeletal Models and Dynamic Simulations: Causes and Effects of Differences Between Models. Annals of Biomedical Engineering, 45 (11), 2635–2647. https://doi.org/10.1007/s10439-017-1894-5

[47] Myers, C. A., Laz, P. J., Shelburne, K. B.; Davidson, B. S. (2015). A Probabilistic Approach to Quantify the Impact of Uncertainty Propagation in Musculoskeletal Simulations. Annals of Biomedical Engineering, 43 (5), 1098–1111. https://doi.org/10.1007/s10439-014-1181-7

[48] Uchida, T. K., Seth, A. (2022) Conclusion or Illusion: Quantifying Uncertainty in Inverse Analyses From Marker-Based Motion Capture due to Errors in Marker Registration and Model Scaling. Front. Bioeng. Biotechnol. 10:874725. doi: 10.3389/fbioe.2022.874725

[49] Charles, J. P., Grant, B., D'Août, K.; Bates, K. T. (2020). Subject-specific muscle properties from diffusion tensor imaging significantly improve the accuracy of musculoskeletal models. Journal of Anatomy, 237(5), 941–959. https://doi.org/10.1111/joa.13261

[50] Akhundov, R., Saxby, D. J., Diamond, L. E., Edwards, S., Clausen, P., Dooley, K., Blyton, S.; Snodgrass, S. J. (2022). Is subject-specific musculoskeletal modelling worth the extra effort or is generic modelling worth the shortcut?. PLoS ONE, 17(1 1). https://doi.org/10.1371/journal.pone.0262936

[51] Puchaud, P., Sauret, C., Muller, A., Bideau, N., Dumont, G., Pillet, H., Pontonnier, C. (2019): Accuracy and kinematics consistency of marker-based scaling approaches on a lower limb model: a comparative study with imagery data, Computer Methods in Biomechanics and Biomedical Engineering, DOI: 10.1080/10255842.2019.1705798

[52] Nolte, D., Tsang, C. K., Zhang, K. Y., Ding, Z., Kedgley, A. E.; Bull, A. M. J. (2016). Non-linear scaling of a musculoskeletal model of the lower limb using statistical shape models. Journal of Biomechanics, 49(14), 3576–3581. https://doi.org/10.1016/j.jbiomech.2016.09.005

[53] Lund, M., Andersen, M., Zee, M., Rasmussen, J. (2015) Scaling of musculoskeletal models from static and dynamic trials, International Biomechanics, 2:1, 1-11, DOI: 10.1080/23335432.2014.993706

[54] de Vet, J. M. (2021). OpenSim upper-extremity modelling: subject-specific scaling-and validation tools. Delft University of Technology, Faculty of 3mE.

[55] Dal Maso, F., Begon, M., Raison, M. (2017). Methodology to customize maximal isometric forces for hill-type muscle models. Journal of Applied Biomechanics, 33(1), 80–86. https://doi.org/10.1123/jab.2016-0062

[56] Correa, T. A., Pandy, M. G. (2011). A mass-length scaling law for modeling muscle strength in the lower limb. Journal of Biomechanics, 44(16), 2782–2789. https://doi.org/10.1016/j.jbiomech.2011.08.024

[57] Goislard de Monsabert, B., Rao, G., Gay, A., Berton, E., Vigouroux, L. (2017). A scaling method to individualise muscle force capacities in musculoskeletal models of the hand and

wrist using isometric strength measurements. Medical and Biological Engineering and Computing, 55(12), 2227–2244. https://doi.org/10.1007/s11517-017-1662-6

[58] Rezzoug, N., Wang, X., Hernandez, V., Gorce, P. (2019). Maximal isometric force exertion predicted by the force feasible set formalism: application to handbraking. Ergonomics, Taylor & Francis, 2019, 62 (12), pp.1551-1562.https://doi.org/10.1080/00140139.2019.1660418

[59] Hernandez, V., Rezzoug, N.; Gorce, P. (2015). Toward isometric force capabilities evaluation by using a musculoskeletal model: Comparison with direct force measurement. Journal of Biomechanics, 48(12), 3178–3184. https://doi.org/10.1016/j.jbiomech.2015.07.003

[60] Hernandez, V., Gorce, P., Rezzoug, N. (2018). Evaluation and validation of musculoskeletal force feasible set indices: Application to manual wheelchair propulsion. Journal of Biomechanics, 68, 70–77. https://doi.org/10.1016/j.jbiomech.2017.12.012

[61] Bolsterlee, B., Alistair, V., Helm, F., Veeger, H. The effect of scaling physiological crosssectional area on musculoskeletal model predictions. Journal of Biomechanics, 48(10):1760–1768, 2015.

[62] How Scaling Works. https://simtk-confluence.stanford.edu:8443/display/OpenSim/How+Scaling+Works

[63] Puchaud, P., Sauret, C., Muller, A., Bideau, N., Dumont, G., Pillet, H., Pontonnier, C. (2020). Accuracy and kinematics consistency of marker-based scaling approaches on a lower limb model: a comparative study with imagery data. Computer Methods in Biomechanics and Biomedical Engineering, 23(3), 114–125. https://doi.org/10.1080/10255842.2019.1705798

[65] Collecting Experimental Data. https://simtk-confluence.stanford.edu:8443/display/OpenSim/Collecting+Experimental+Data.

[66] Modenese, L., Montefiori, E., Wang, A., Wesarg, S., Viceconti, M., Mazzà, C. (2018). Investigation of the dependence of joint contact forces on musculotendon parameters using a codified workflow for image-based modelling. Journal of Biomechanics,73, 108–118. https://doi.org/10.1016/j.jbiomech.2018.03.039

[67] OpenSim::MocoInverse Class Reference.OpenSim Moco 0.2.0. https://opensim-org.github.io/opensim-moco-site/docs/0.2.0/class_open_sim_1_1_moco_inverse.html

[68] OpenSim::MocoMarkerTrackingGoal Class Reference.OpenSim Moco 0.2.0. https://opensim-org.github.io/opensim-moco-site/docs/0.2.0/class_open_sim_1_1_moco_marker_tracking_goal.html

[69] J. Blank and K. Deb (2020). pymoo: Multi-Objective Optimization in Python, in IEEE Access, vol. 8, pp. 89497-89509, 2020, doi: 10.1109/ACCESS.2020.2990567

[70] Sensor Locations. http://www.seniam.org/

[71] AVIA semiconductor. HX711. 24-Bit Analog-to-Digital Converter (ADC) for Weigh Scales. https://cdn.sparkfun.com/datasheets/Sensors/ForceFlex/hx711_english.pdf

[72] ArduinoTM UNO. Arduino UNO Reference Design. https://www.arduino.cc/en/uploads/Main/arduino-uno-schematic.pdf

[73] Mira, R., Tosatti, L., Sacco, M., Scano, A. (2021). Detailed characterization of physiological EMG activations and directional tuning of upper-limb and trunk muscles in point-to-point reaching movements. Institute of Intelligent Industrial Technologies and Systems for Advanced Manufacturing (STIIMA), National Research Council of Italy (CNR), 23900, Lecco, Italy. Current

Research in Physiology, Volume 4,2021,Pages 60-72, ISSN 2665-9441, https://doi.org/10.1016/j.crphys.2021.02.005.

[74] IFTOOLS GmbH. The clever Terminal for field-bus applications. https://www.iftools.com /tools/cleverterm/index.en.php

[75] Weight of Human Body Parts. https://robslink.com/SAS/democd79/body_part_weig hts.htm

[76] MocoInverse: solving muscle and actuator redundancy. https://opensim-org.github.io/opensim-moco-site/docs/